ACS OMEGA

http://pubs.acs.org/journal/acsodf

Article

Multitargeting Antibacterial Activity of a Synthesized Mn^{2+} Complex of Curcumin on Gram-Positive and Gram-Negative Bacterial Strains

Tanmoy Saha,[‖] Prince Kumar,[‖] Nayim Sepay, Durba Ganguly, Kanchan Tiwari, Kasturi Mukhopadhyay,* and Saurabh Das*

Cite This: *ACS Omega* 2020, 5, 16342−16357

Read Online

ACCESS | Metrics & More | Article Recommendations | Supporting Information

ABSTRACT: Curcumin is an important molecule with a plethora of pharmacological activities and therapeutic potentials. Despite its efficacy, it remained a potential drug candidate owing to hydrolytic instability and poor aqueous solubility. To overcome the limitations related to low solubility, low bioavailability, and the fact that curcumin is never present in solution as a "single unit", its complex was prepared with Mn^{II} with the idea that binding to a metal ion might help to resolve these issues. The complex was characterized by elemental and spectral analysis. The structure of the complex was determined by density functional theory calculations. The complex was stable at physiological buffer conditions, unlike curcumin. It did not have any detrimental effect on mammalian cells. There was a significant enhancement in the antibacterial activity of the complex compared to curcumin against both Gram-positive (*Staphylococcus aureus*) and Gram-negative (*Escherichia coli*) bacteria. It showed a strong affinity for deoxyribonucleic acid (DNA) evident from a high binding constant value with calf thymus DNA and also from the retarded electrophoretic mobility of bacterial plasmid DNA. The complex showed "superoxide dismutase-like" activity leading to the generation of reactive oxygen species (ROS). The complex caused bacterial membrane perturbation evident from calcein leakage assay, which was further corroborated by scanning and transmission electron microscopic experiments. Overall, the present study shows improved stability and antibacterial potency of a nontoxic complex over curcumin. Its multitargeting mode of action such as ROS-production, effective binding with DNA, and permeabilization of bacterial membrane together allows it to be an effective antibacterial agent that could be taken further for therapeutic use against bacterial infections.

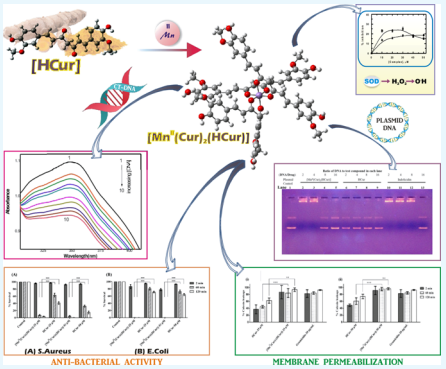

1. INTRODUCTION

Curcumin (HCur) [1,7-bis(4-hydroxy-3-methoxyphenyl)-hepta-1,6-dienne-3,5-dione], the yellow pigment extracted from turmeric (*Curcuma longa* Linn), is a well-known lipophilic polyphenolic compound.[1−4] Besides its traditional use as a cooking ingredient in many Asian communities, it has been an integral component of Ayurveda and used in wound healing, common cold, fever, inflammation, arthritis, and so forth.[1−5] Although known for a long time, it gained considerable attention in the last few decades when numerous studies established that HCur possesses many pharmacological properties that include antitumor, anti-inflammatory, antioxidant, and antiviral applications in neuro-degenerative diseases.[2−9] Moreover, the excellent potency of HCur is associated with its safe toxicity profile, as clinical trials have shown it to be safe even at high oral doses of 12 g per day.[10] In addition to its plethora of pharmacological properties, HCur also possesses antimicrobial activity against a wide range of micro-organisms.[11] Earlier, we have reported that HCur is highly effective against both Gram-positive and Gram-negative bacterial strains under *in vitro* conditions.[12] However, its full potential as a therapeutic agent could not be achieved owing to poor physiological stability and low aqueous solubility, resulting in poor bioavailability.[13−15]

HCur is a symmetrical molecule showing a dynamic keto−enol tautomerism because of the β-diketone moiety. The presence of β-diketone is probably a reason for its hydrolytic instability in cellular medium, resulting in poor bioavailability.[13,16] In fact, HCur undergoes rapid degradation in different physiological buffers as well as in different cell culture media, although in the latter, it is slightly more stable because of the presence of serum proteins.[17,18] Therefore, to address the issue of stability, considered a serious disadvantage, a complex was prepared with Mn^{II}.[19] Complexes of Mn^{II} with HCur were prepared earlier, but the one which we prepared was different in terms of composition.[19−21] Phenolic −OH groups that are centers of potential activity often lead to

Received: November 30, 2019
Accepted: June 16, 2020
Published: July 6, 2020

https://dx.doi.org/10.1021/acsomega.9b04079
ACS Omega 2020, 5, 16342−16357

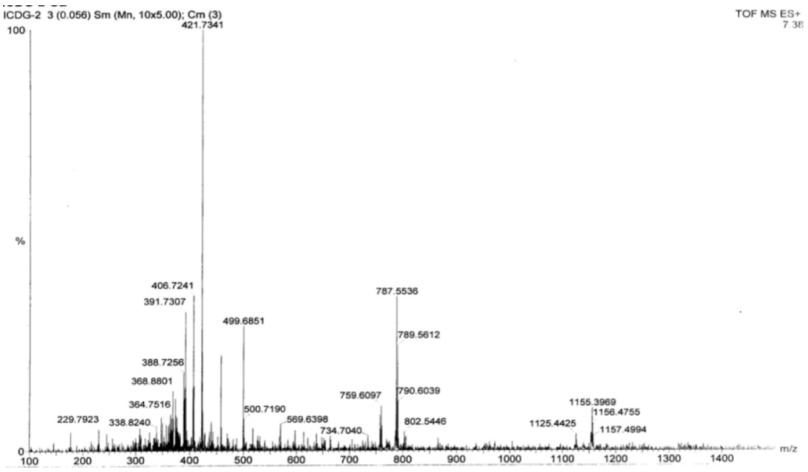

Figure 1. Mass spectra of the Mn^{II} complex of HCur.

complications during complex formation, forming insoluble polymeric species.[7,9,14−16,19,22] However, when prepared with precaution, coordination complexes of HCur possess different biological attributes that can be used to an advantage.[16,23−25] In the present investigation, a Mn^{II}−HCur complex was prepared and characterized by elemental and spectral analysis and its electronic structure was established by density functional theory (DFT) calculations. We then investigated the hydrolytic stability of the complex in different biological milieu to find out if complex formation with Mn^{II} improves stability. It was studied for its superoxide dismutase (SOD)-like activity, resulting in the generation of reactive intermediates and interaction with deoxyribonucleic acid (DNA). Further, its antibacterial activity was investigated against clinically significant Gram-positive (*Staphylococcus aureus*) and Gram-negative (*Escherichia coli*) bacteria. These are among the most prevalent and most common causes of hospital- and community-acquired infections. *S. aureus* is an opportunistic pathogen causing several life-threatening diseases such as osteomyelitis, endocarditis, and toxic shock syndrome.[26] According to the Broad Institute, *E. coli* accounts for 17.3% of clinical infections requiring hospitalization and happens to be the second most common source of infection behind *S. aureus* (18.8%). In Gram-negative bacteria, there is an additional layer of protection of the outer membrane of lipopolysaccharides (LPSs), allowing them to resist most of the traditional antibiotics and making Gram-negative bacteria more dangerous in hospital settings.

Next, to decipher the mechanism behind the superior antibacterial activity of the complex over HCur, we assessed the ability to permeabilize the cytoplasmic membrane of the bacteria using the fluorescence-based calcein leakage assay. We also examined the affinity of the complex toward LPSs of *E. coli* using BODIPY-TR-cadaverine displacement assay. These membrane-targeting modes of action were further confirmed by microscopic visualization. Further, to rationalize the therapeutic potential of the complex, its toxic effects on mammalian cells were evaluated.[27,28]

2. RESULTS AND DISCUSSION

2.1. Characterization of the Complex. Owing to poor solubility in water, the spectrum of the complex was recorded in dimethyl sulfoxide (DMSO) (Figure S1, Supporting Information). λ_{max} obtained at 400 nm in DMSO (molar extinction coefficient ε = 2.85 × 10^4 M^{-1} cm^{-1}) was comparable to the spectrum recorded during physicochemical experiments where Mn^{II} and HCur were allowed to interact with each other, showing peaks at 430 nm in aqueous−ethanol medium (Figure S2, Supporting Information). The Fourier transform infrared (FTIR) spectrum of HCur (Figure S3, Supporting Information), recorded on a PerkinElmer spectrometer (Spectrum Two) with samples by use of the attenuated total reflection technique, indicates a peak at 3516 cm^{-1} owing to −OH stretching, which for the complex was observed as a broad band at 3403 cm^{-1} (Figure S4, Supporting Information).[29] Sharp peaks at 1627 and 1604 cm^{-1}, attributed to C═O stretching vibrations in HCur, got shifted to lower wavenumbers (1581 and 1516 cm^{-1}, respectively) in the complex having low intensities, suggesting involvement of the carbonyl group in binding Mn^{II}. Peaks at 1506 and 1429 cm^{-1} due to C═C stretching and C═O bending vibrations in the IR spectrum of HCur also showed significant changes in the complex.[29]

The mass spectrum was recorded on a Micromass Q-TOF Micro, Waters Corporation. Analysis of mass spectrometry data was done considering a 1:3 complex formed between Mn^{II} and HCur (Figure 1). The molecular ion peak was obtained in a cluster of peaks having m/z 1157.4994, 1156.4755, and 1155.3969 [m/z (theo) = 1157.3004]. From the molecular ion, loss of one ligand has Mn^{II} bound to two curcumins. Both curcumins could be bound as enolate (expected m/z = 789.1743) or one could be bound in the enolate form and the other as a diketone (expected m/z = 790.1822). Hence, peaks obtained at m/z = 790.6039, 789.5612, and 787.5536 (expected m/z −2H) support formation of such fragments.

Loss of two ligands from the molecular ion should form a 1:1 metal/ligand fragment with expected peaks at m/z = 422.0562 (if enolate) and 423.0640 (if diketo). Appearance of a peak at m/z = 421.7341 indicates formation of this fragment. Peaks at m/z = 364.7516 and 368.8801 indicate free HCur released by the complex during analysis. Therefore, the mass spectrum of the complex provides good evidence in favor of a 1:3 metal to ligand stoichiometry.

Thermogravimetric analysis (TGA) of the complex performed on a Mettler Toledo TGA/SDTA 851 (Figure S5, Supporting Information) shows up to 100 °C; there is no appreciable loss in weight. Considering the initial weight at 28 °C to be 15.4364 mg, the weight recorded at ∼196 °C was

https://dx.doi.org/10.1021/acsomega.9b04079
ACS Omega 2020, 5, 16342−16357

14.2364 mg. Hence, loss in weight was 1.2 mg. Percentage loss in weight (7.774%) corresponds to the loss of three $-OCH_3$ groups from the complex, probably one from each ligand (theoretical loss = 7.772%). At 280 °C, the weight recorded was 13.0463 mg. Hence, loss in weight and percentage loss were 2.3901 mg and 15.483%, respectively. This loss in weight corresponds to the loss of six $-OCH_3$ groups from the complex, that is, two from each ligand (theoretical loss = 15.543%). Hence, TGA data also suggest the formation of a 1:3 complex. The molar conductance of the complex in pure DMSO was determined on a conductivity meter EUTECH CON 700, Thermo Scientific, Eutech Instruments and found to be 15.2 S m^2 mol^{-1}, suggesting it to be a nonelectrolyte in solution. We tried to obtain single crystals of the prepared complex but were not successful. Hence, we tried to obtain a structure from DFT based on spectroscopic evidence. The obtained structure has good correlation with experimental data. Magnetic susceptibility measurements of powdered samples at room temperature (298 K) were done by the Gouy method on Magway MSB MK1, Sherwood Scientific Ltd. The μ_{eff} was found to be 6.06 BM.

2.2. Optimization of Molecular Geometry and Electronic Structure. The geometries of both the ligand and the complex were optimized using DFT. What transpired from the DFT study is that Mn^{II} forms an octahedral complex with curcumin with two molecules of it coordinating the metal center as enolate anion (Cur) and one coordinating it in the diketo form (HCur). The ground-state optimized geometry of the ligand and its Mn^{II} complex are shown in Figure 2.

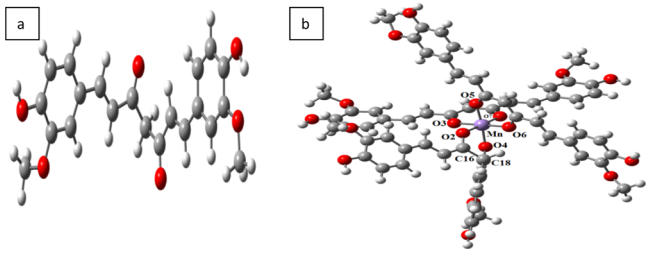

Figure 2. Optimized geometry of (a) HCur and (b) $[Mn^{II}(Cur)_2(HCur)]$.

Optimized geometrical parameters of the complex are listed in Table 1. The model geometry possesses a distorted octahedral arrangement around Mn^{II}. Calculated Mn−O distances were found in the expected range of 1.869−1.926 Å.[30] Hence, DFT calculations unequivocally support the formation of an octahedral Mn^{II} complex. If we consider the coordination environment around Mn^{II} (Figure 2b), O5 and O6 belong to one ligand, O3 and O7 to a second ligand, and O2 and O4 are from a third ligand. Interestingly, Mn−O bond lengths (Table 1) suggest that Mn−O2 and Mn−O4 are slightly longer than the other four (i.e., Mn−O3, Mn−O7, Mn−O5, Mn−O6), indicating that coordination by oxygen donor sites from two ligands are of one type and that from the third ligand is slightly different.

This fact is supported experimentally by the conductance measurement data (reported in Section 2.1) that had suggested the complex to be a nonelectrolyte. In other words, the calculated Mn−O bond distance data suggesting binding of two curcumins to Mn^{II} as enolate anions and one as diketone explain the formation of a neutral complex that correlated with

Table 1. Selected Optimized Geometrical Parameters for a Complex in Ground State Calculated at LANL2DZ Levels for the Metal and 6-31G Levels for the Atoms C, H, and O

bond type	bond length (Å)
Mn−O2	1.926
Mn−O3	1.889
Mn−O4	1.900
Mn−O5	1.869
Mn−O6	1.882
Mn−O7	1.884
bond angle	value (deg)
O2−Mn−O3	87.30
O2−Mn−O4	89.01
O2−Mn−O5	87.90
O2−Mn−O6	90.53
O2−Mn−O7	178.34
O3−Mn−O4	88.74
O3−Mn−O5	87.67
O3−Mn−O6	177.84
O3−Mn−O7	91.59
O4−Mn−O5	175.37
O4−Mn−O6	91.16
O4−Mn−O7	92.21
O5−Mn−O6	92.33
O5−Mn−O7	90.81
O6−Mn−O7	90.58
C16−C18−C17	105.69

the experimental data (obtained from conductance) as one of a nonelectrolyte.

From the data in Table 1, it can be said that those oxygen coordinations with a slightly larger Mn−O bond length have curcumin coordinating Mn^{II} in the diketo (neutral) form, denoted as HCur in the formula. The other four oxygen coordinations of Mn^{II} showing an almost similar Mn−O bond length have curcumin coordinating the metal center as enolate anions (denoted in the formula as Cur). Further, we also found from the DFT calculated structure that in case of curcumin while coordinating Mn^{II} in the diketo form, carbon−oxygen bond distances are slightly shorter (as expected) than the other four carbon−oxygen bond distances where they coordinate as enolate anions. When coordination occurs because of resonating C═O and $C-O^-$ forms as for any enolate anion, carbon−oxygen bond distances are likely to be slightly larger than when it is a diketo coordination (Figure S6, Supporting Information). This was actually found for this complex, suggesting that curcumin coordinating Mn^{II} through O2 and O4 does so as diketo, following which their corresponding carbon−oxygen bond distances (C16−O2 and C17−O4) were slightly shorter (Table S1, Supporting Information). Our values may be compared with a 1:1 Mn^{II}/curcumin complex reported earlier where the structure was also arrived at with DFT calculations.[31]

For HCur in its ground state, the electron densities of the highest occupied molecular orbitals (HOMO) and the lowest unoccupied molecular orbitals (LUMO) reside mainly over the benzene ring. The energy difference between HOMO and LUMO was found to be 3.55 eV (Figure 3). This assignment is supported by time-dependent DFT (TD-DFT) calculations. For the complex, the LUMO, LUMO + 1, and HOMO originate from symmetry orbitals of ligands with contribution from Mn d orbitals. The energy difference between HOMO

https://dx.doi.org/10.1021/acsomega.9b04079
ACS Omega 2020, 5, 16342−16357

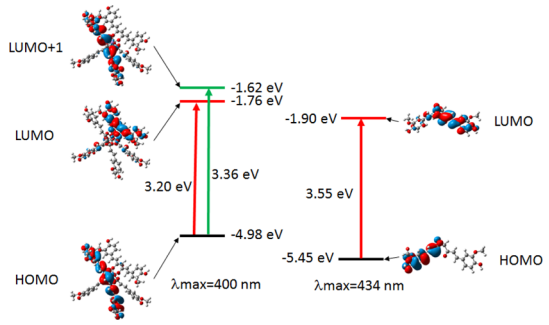

Figure 3. Frontier molecular orbitals involved in the UV−vis absorption of the ligand and the metal complex.

and LUMO in the complex was found to be 3.36 and 3.20 eV, respectively.

2.3. Analysis for Stability of the Complex in Different Media by UV−Visible Spectroscopy. Considering the facts that are known pertaining to the instability of HCur, we examined the stability of $[Mn^{II}(Cur)_2(HCur)]$ in different biological milieu (Figures S7 and S8, Supporting Information).[18] As seen from different figures, in contrast to HCur, there were no changes in the absorbance intensity of the complex (Figures S7 and S8, Supporting Information) in a biological buffer and microbiological media. Worth noting is the fact that HCur is more stable in microbiological media (Figure S8, Supporting Information) compared to phosphate-buffered saline (PBS) buffer. As the environment for most cellular compartments is reducing in nature, the stability of HCur and $[Mn^{II}(Cur)_2(HCur)]$ was investigated in the presence of dithiothreitol (DTT), a strong reducing agent.[32] HCur lost 50% of its absorption intensity within 5 min of coincubation with DTT, whereas no change was observed in the spectrum of $[Mn^{II}(Cur)_2(HCur)]$ even after 20 min of incubation. As evident from Figures S7 and S8, Supporting Information, the complex is stable in physiological buffer and media even under reducing conditions.

2.4. Interaction of $[Mn^{II}(Cur)_2(HCur)]$ with Calf Thymus DNA. The complex was titrated with calf thymus DNA at constant pH (=7.4) and constant ionic strength of the

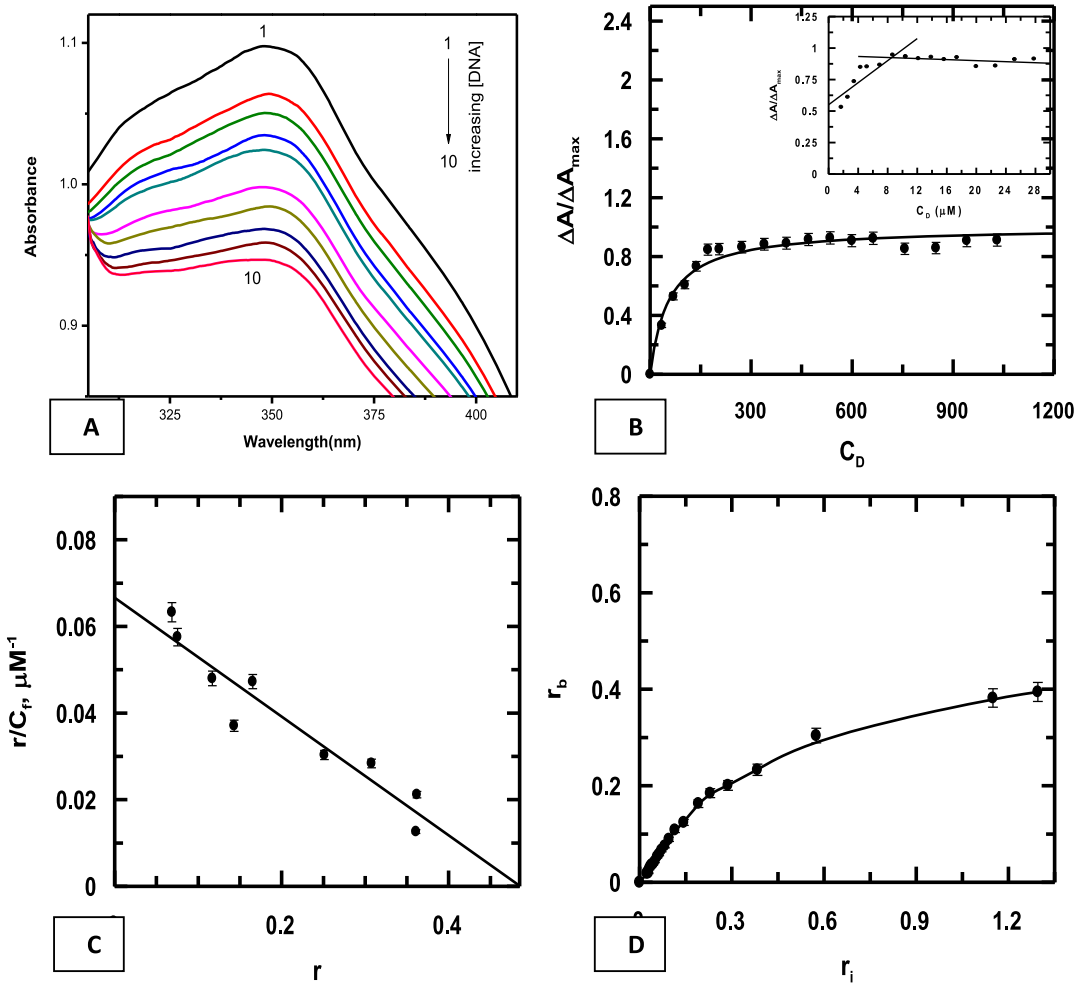

Figure 4. (A) Absorption spectra of $[Mn^{II}(Cur)_2(HCur)]$ in the absence (1) and presence of different concentrations of calf thymus DNA (2) 62.65, (3) 124.69, (4) 246.94, (5) 307.16, (6) 599.69, (7) 851.32, (8) 1092.60, (9) 1248.02, and (10) 1399.30 μM; (B) binding isotherm for $[Mn^{II}(Cur)_2(HCur)]$ interacting with calf thymus DNA when $\Delta A/\Delta A_{max}$ was plotted against the concentration of DNA; the dark line indicates the fitted data obeying eq 4. Inset: Plot of normalized increase in absorbance as a function of mole-ratio of calf thymus DNA to $[Mn^{II}(Cur)_2(HCur)]$; (C) modified Scatchard plot for the interaction of $[Mn^{II}(Cur)_2(HCur)]$ with calf thymus DNA; (D) plot of input $[Mn^{II}(Cur)_2(HCur)]$/DNA ratio (r_i) to bound $[Mn^{II}(Cur)_2(HCur)]$/DNA ratio (r_b) as calculated from the decrease in absorbance following interaction of $[Mn^{II}(Cur)_2(HCur)]$ with calf thymus DNA; $[Mn^{II}(Cur)_2(HCur)]$ = 40 μM, [NaCl] = 150 mM, pH = 7.4, temp. = 298 K.

https://dx.doi.org/10.1021/acsomega.9b04079
ACS Omega 2020, 5, 16342−16357

Table 2. Binding Constant Values for Interaction of the Complex with the Calf Thymus DNA

apparent binding constants $K_{app} \times 10^{-4}$ (M^{-1})				overall binding constant ($K' \times 10^{-5}$ M^{-1}) $K' = K_{app} \times n_b$			
from double reciprocal plot eq 2	from nonlinear fit eq 4	from double reciprocal plot with y-intercept = 1 eq 5	site size (n_b) from mole ratio plot	using K_{app} from eq 2	using K_{app} from eq 4	using K_{app} from eq 5	overall binding constant $K' \times 10^{-5}$ (M^{-1}) (by the Scatchard plot, eq 6)
4.10	6.87	2.10	8.0	3.28	5.50	1.68	1.26

medium (0.15 mM).[33−35] Titrations showed a gradual decrease in absorbance at 367 nm, which was used to follow the interaction of $[Mn^{II}(Cur)_2(HCur)]$ with calf thymus DNA (Figure 4A). Figure S9, Supporting Information, is a plot of $1/\Delta A$ versus $1/[C_D - C_L]$ (eq 2) that provides a value for apparent binding constant [K_{app} ($=K_d^{-1}$)]. Titrations were repeated thrice. The values obtained were in the range of 2.73×10^4 to 5.47×10^4 M^{-1}.[33,35−39] Figure 4B is a plot of $\Delta A/\Delta A_{max}$ versus concentration of calf thymus DNA. Nonlinear curve fitting was applied (eqs 3 and 4) on three separate titrations and an average apparent binding constant ($K_{app} = 6.87 \times 10^4$ M^{-1}) were evaluated.[33,35−39] The inset of Figure 4B provides a value for n_b (=8.0), the number of nucleotides bound to the complex following its interaction with calf thymus DNA.

The titration data were also fitted to eq 5 that plots the inverse of the fraction of the complex bound to the calf thymus DNA to the inverse of the concentration of the calf thymus DNA used in the experiment.[33,36−39] The inverse of the slope of the plot (Figure S10, Supporting Information) provides yet another value of apparent binding constant. An average of K_{app} from eq 5 obtained from three separate titrations was 2.10×10^4 M^{-1}. Apparent binding constants obtained from three different approaches (eqs 2−5) when multiplied with n_b provide the overall binding constant (K') [Table 2]. Data from the titration were also fitted to a modified form of the Scatchard equation (Figure 4C).[40] K' and n ($=n_b^{-1}$) were obtained. "n" denotes the number of complex molecules bound to a nucleotide. Figure 4D relates the ratio of the input drug/DNA (r_i) to the ratio of the bound drug/DNA (r_b) as derived from Scatchard calculations.[41] For such a plot, a 45° line passing through the initial points indicates that the entire compound was eventually bound to the DNA.[41]

2.5. Hypoxanthine to Xanthine/Xanthine Oxidase-Inhibiting Activity of $[Mn^{II}(Cur)_2(HCur)]$. Xanthine oxidase is an enzyme that generates reactive oxygen species (ROS) by catalyzing the oxidation of hypoxanthine to xanthine and then of xanthine to uric acid.[42,43] As xanthine oxidase is a superoxide-producing enzyme, it was used in an assay where depletion of superoxide was followed by reduction of nitro-blue tetrazolium dichloride (NBT^{2+}) having an affinity for it. The assay indicates that $[Mn^{II}(Cur)_2(HCur)]$ has SOD-like activity, that is, it assists in disproportionation of a superoxide radical anion to molecular oxygen and hydrogen peroxide (Figure 5).

Thus, such formation of H_2O_2 in the system where $[Mn^{II}(Cur)_2(HCur)]$ is present is important as it leads to the generation of a hydroxyl radical ($HO^•$) known for its ability to cause oxidative stress. Therefore, this provides another reason why the complex shows improved antibacterial activity reported and discussed in the following sections.[44−46] In this regard, it should however be mentioned (as correctly pointed out by one reviewer while reviewing this manuscript) that although we consider formation of the hydroxyl radical ($HO^•$) as logically formed from H_2O_2 and use it to explain the better performance of the complex in comparison to curcumin, it would have been nice had we shown its actual formation by the deoxyribose assay, which, for more than one reason, could not be included in our study.[47,48]

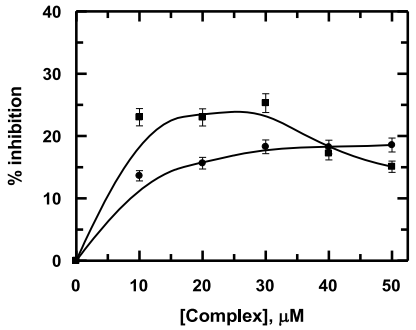

Figure 5. Percentage inhibition of a superoxide radical anion formed because of the hypoxanthine/xanthine oxidase enzyme assayed by NBT^+ absorption at 524 nm in the presence of $[Mn^{II}(Cur)_2(HCur)]$ (■) and SOD (●); 50 μM hypoxanthine, 0.04 unit of xanthine oxidase, 300 μM NBT^{2+} and 10% DMSO.

2.6. Antibacterial Activity of $[Mn^{II}(Cur)_2(HCur)]$ on *S. aureus* and *E. coli*. The antibacterial efficacy of $[Mn^{II}(Cur)_2(HCur)]$ was compared to that of HCur against *S. aureus* ATCC 29213 and *E. coli* ATCC 25922 with the help of a killing assay, exposing cells (10^6 cfu/mL) to two different concentrations (25 and 50 μM) and plating aliquots on a brain heart infusion (BHI) agar plate at selected time intervals. The percentage survival of $[Mn^{II}(Cur)_2(HCur)]$- and HCur-treated bacterial cells was calculated after comparing with untreated control (Figure 6A,B). Bacterial survival is also presented in the logarithmic scale as $\log_{10}$ cfu/mL in the Supporting Information (Figure S11, Supporting Information). The complex $[Mn^{II}(Cur)_2(HCur)]$ showed a significant (p-value ≤ 0.001) improvement in antibacterial activity compared to HCur against both *S. aureus* and *E. coli*. As seen from the killing assay of *S. aureus* in Figure 6A, exposure of 25 μM $[Mn^{II}(Cur)_2(HCur)]$ for 60 min caused 92.90 ± 1.87% killing, whereas a similar exposure of HCur could kill only 36.68 ± 5.13% cells. Upon increasing the concentration to 50 μM, $[Mn^{II}(Cur)_2(HCur)]$ caused 95.58 ± 2.08% killing, whereas a similar increase for HCur killed 67.48 ± 2.77% in 60 min.

Exposure of 50 μM $[Mn^{II}(Cur)_2(HCur)]$ for 120 min showed 99.68 ± 0.12% killing, whereas 85.04 ± 3.94% killing was observed with HCur (Figure 6A). In the log-scale representation, exposure of 50 μM $[Mn^{II}(Cur)_2(HCur)]$ for 120 min caused 2.52 ± 0.15 $\log_{10}$ cfu/mL reduction, whereas a similar concentration of HCur caused only 0.78 ± 0.13 $\log_{10}$ cfu/mL reduction in an initial cell count of 5.76 ± 0.02 $\log_{10}$ cfu/mL cells (Figure S11, Supporting Information). Further, a killing assay on *E. coli*, presented in Figure 6B, showed a much more prominent antibacterial effect by the complex than HCur. Exposure of 25 μM of $[Mn^{II}(Cur)_2(HCur)]$ for 60 min showed 99.72 ± 0.05% cell killing, whereas a similar exposure

https://dx.doi.org/10.1021/acsomega.9b04079
ACS Omega 2020, 5, 16342−16357

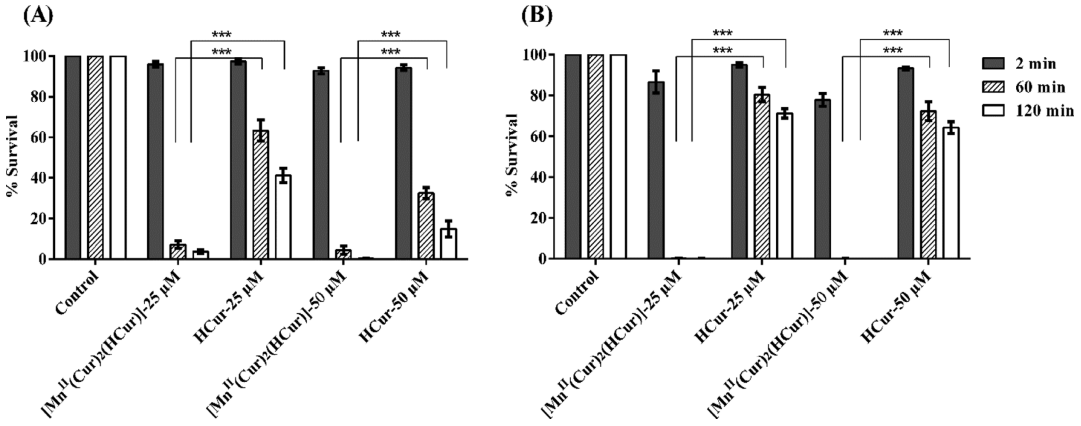

Figure 6. Antibacterial efficacy of 25 and 50 μM of $[Mn^{II}(Cur)_2(HCur)]$ and HCur in PBS buffer against (A) *S. aureus* and (B) *E. coli* cells ($\sim 10^6$ cfu/mL). Gray columns, columns with stripes, and white columns denote the time of exposure (2, 60, and 120 min, respectively) to the compounds. The data represent mean ±SD)of three independent experiments (***$p \leq 0.001$).

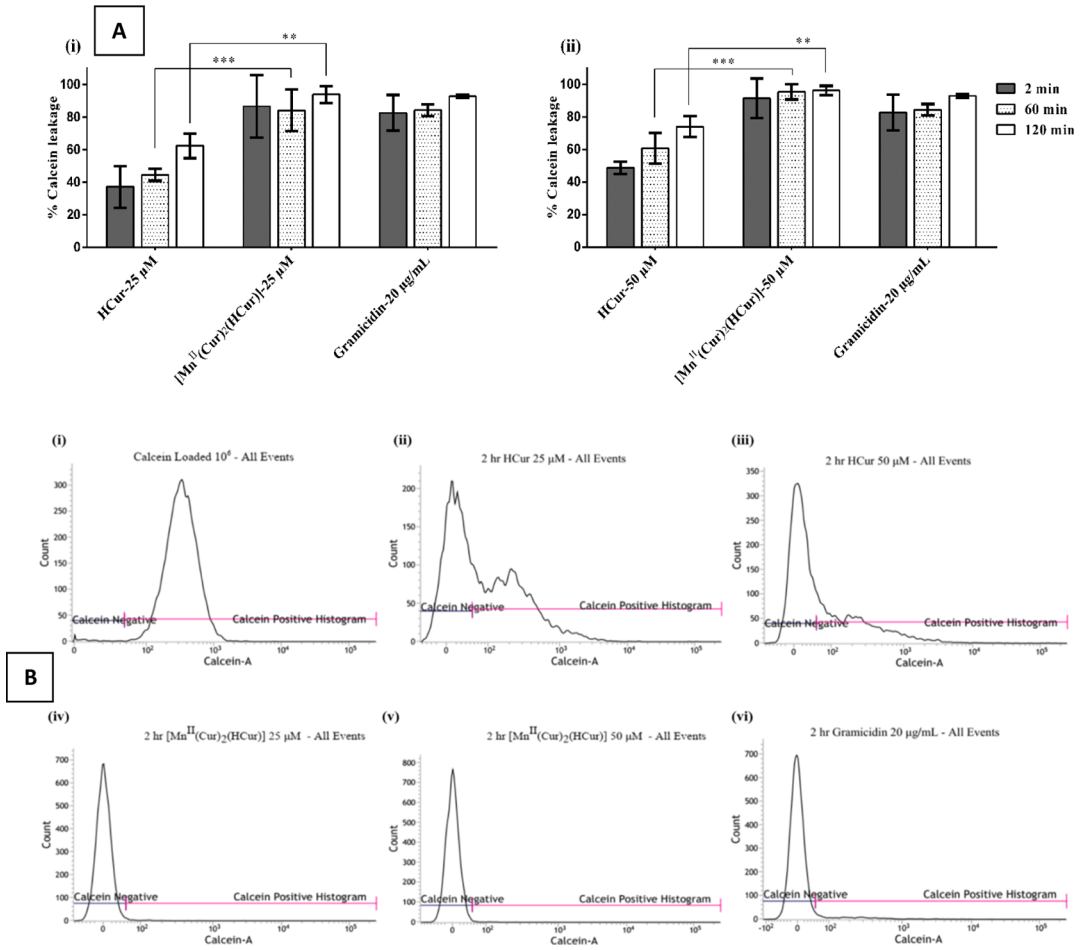

Figure 7. (A) Percentage of calcein leakage from bacterial cells caused by 25 and 50 μM $[Mn^{II}(Cur)_2(HCur)]$ and HCur upon exposure of 2, 60, and 120 min of incubation. (B) Representative histograms of calcein-loaded cells incubated with 25 and 50 μM $[Mn^{II}(Cur)_2(HCur)]$ and HCur for 120 min. A total of 10,000 cells were acquired for each flow cytometry analysis. The data represent the mean ±SD of three independent experiments (**$p \leq 0.01$, ***$p < 0.001$).

of HCur killed only 19.59 ± 3.63% cells. Even after increasing the concentration and exposure time to 50 μM and 2 h, respectively, HCur could kill only 35.69 ± 2.82% cells, whereas under similar conditions, $[Mn^{II}(Cur)_2(HCur)]$ caused 100% killing. In the log scale, there was no observable reduction in $\log_{10}$ cfu/mL compared to the control even after increasing the concentration and exposure time to 50 μM and 120 min for HCur. However, under similar conditions, the complex caused 4.02 ± 0.67 $\log_{10}$ cfu/mL in an initial cell count of 5.49 ± 0.24 $\log_{10}$ cfu/mL (Figure S11, Supporting Information).

Overall, the killing efficacy of the complex $[Mn^{II}(Cur)_2(HCur)]$ was found to be significantly (p-value

https://dx.doi.org/10.1021/acsomega.9b04079
ACS Omega 2020, 5, 16342−16357

$\leq$ 0.001) better than HCur in both *S. aureus* and *E. coli* in all tested conditions.

2.7. Mechanism of Antibacterial Action Due to the Complex. *2.7.1. Membrane Permeabilization of S. aureus by Calcein Leakage.* Toward deciphering the mechanism behind the antibacterial activity of $[Mn^{II}(Cur)_2(HCur)]$, its ability to permeabilize bacterial membranes was studied by calcein leakage assay using flow cytometry.[12,49,50] Bacterial cells were exposed to two different concentrations of HCur and $[Mn^{II}(Cur)_2(HCur)]$, that is, 25 and 50 μM, respectively. The results presented in Figure 7A(i) show 25 μM $[Mn^{II}(Cur)_2(HCur)]$ caused 86.71 $\pm$ 19.19% dye leakage for a 2 min incubation as compared to HCur causing only 37.22 $\pm$ 12.81%. Incubation of 50 μM HCur for 120 min showed 73.93 $\pm$ 11.16% dye leakage, whereas exposure to the same time and a similar concentration of $[Mn^{II}(Cur)_2(HCur)]$ caused a dye leakage of 96.19 $\pm$ 4.95%, comparable to 20 μg/mL gramicidin-D (92.8 $\pm$ 1.78%) [Figure 7A(ii)]. Overall, the complex showed a better membrane permeabilization activity than HCur. In fact, the extent of permeabilization by the complex was almost equal to that of the well-known pore-forming peptide gramicidin-D. Figure 7B shows histograms of calcein-loaded cells incubated with 25 and 50 μM HCur and $[Mn^{II}(Cur)_2(HCur)]$ for 120 min. The loss in calcein fluorescence as a result of membrane permeabilization for $[Mn^{II}(Cur)_2(HCur)]$-treated samples was found to be statistically significant compared to HCur at time intervals of 60 min (p-value < 0.001) and 120 min (p-value < 0.01) of incubation, respectively.

2.7.2. Binding Affinity of the Complex with LPS. As LPS is the major constituent of the outer membrane of Gram-negative bacteria, we examined the ability of the complex to bind to LPS, using a fluorescence-based displacement assay with BODIPY-TR-cadaverine.[51] As shown in Figure 8, there was a

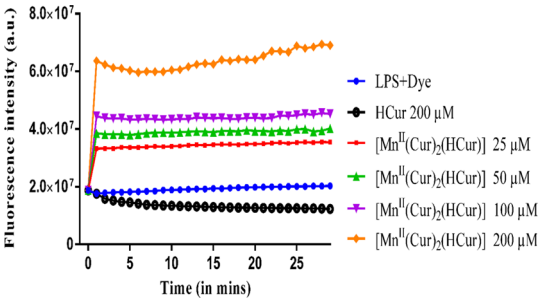

Figure 8. Binding affinity of compounds to LPSs determined by the BODIPY-cadaverine displacement method. Representative data of LPS binding of the complex (25, 50, 100, and 200 μM) and 200 μM of HCur for 30 min are presented here.

rapid increase in fluorescence intensity in a dose-dependent manner. Increase of dye fluorescence reflected its dequenching because of its displacement by the complex from LPS, suggesting that the complex has a marked affinity toward LPSs, whereas the parent molecule (HCur) does not bind to LPSs even at the highest tested concentration of 200 μM. Therefore, LPS binding and calcein leakage assay collectively suggested that the complex first binds to LPSs, which leads to disruption of the *E. coli* outer membrane and then it induced permeabilization of the inner membrane.

2.7.3. Evaluation of Membrane Damage in S. aureus Using Fluorescence Microscopy. To assess the membrane integrity and bacterial cell viability, a mixture of two DNA-binding fluorescent probes SYTO 9 and propidium iodide (PI) were used. SYTO 9 is a green fluorescent stain that generally labels all bacterial cells. In contrast, PI is a red fluorescent stain with stronger binding affinity for DNA compared to SYTO 9 and penetrates only those cells having a damaged membrane. When both dyes are present, it is possible to replace SYTO 9 from DNA, causing a decrease in SYTO 9 (green) fluorescence.[12,52]

A fluorescein isothiocyanate (FITC) filter (green) corresponding to SYTO 9 and a PI filter (red) were followed by a bright field under 60× objective and used to visualize the samples treated with 50 μM $[Mn^{II}(Cur)_2(HCur)]$ and HCur, which were subsequently compared with untreated cells taken as control. The representative merged image of both channels (FITC + PI) is presented in Figure 9. As clearly evident from Figure 9A, untreated control cells appeared predominantly green, indicating that cells are viable and the membrane intact. However, $[Mn^{II}(Cur)_2(HCur)]$-treated cells appeared predominantly red, indicating a loss in membrane integrity and viability of cells (Figure 9B). Cells treated with HCur appeared to be having a mixed population of green, red, and yellow (where both red and green dyes were retained) (Figure 9C). This might be due to minor damages in the membrane allowing only some PI to enter the cells, which is not sufficient to replace all SYTO 9 from DNA. Thus, such cells appear green and yellow.

2.7.4. Morphological Changes in S. aureus Observed by a Scanning Electron Microscope. To further assess if $[Mn^{II}(Cur)_2(HCur)]$ is able to perturb the surface integrity of *S. aureus* ATCC 29213, the cells were visualized by scanning electron microscopy (SEM) following treatment. As shown in Figure S12A, Supporting Information, untreated cells looked bright, smooth, and having an intact surface with round morphology. However, in cells that were treated with 50 μM $[Mn^{II}(Cur)_2(HCur)]$ and HCur, surface perturbation was evident. These cells had an irregular shape with a dent or depression on the surface, along with the appearance of blebs with a rough surface (Figure S12B,C, Supporting Information). Loss of surface morphology and release of intracellular content as debris for complex-treated cells was comparable to cells treated with 20 μg/mL gramicidin D (Figure S12D, Supporting Information).

2.7.5. Ultrastructural Changes in S. aureus Observed by a Transmission Electron Microscope. Further, ultrastructural changes in the cell wall and membrane of *S. aureus* ATCC 29213 cells were examined by transmission electron microscopy (TEM) after 2 h of exposure with 50 μM $[Mn^{II}(Cur)_2(HCur)]$ and HCur. As evident from Figure 10A, untreated control cells had an intact surface with intact cell wall and membrane. However, following treatment with $[Mn^{II}(Cur)_2(HCur)]$, the membrane architecture and surface integrity were severely compromised, with most cells being irregularly shaped. Many cells (ghost cells) lacked cytoplasmic content and were devoid of a cell wall, whereas few of the cells had shredded cell walls and a membrane through which intracellular content oozed out (Figure 10B,C). The results are comparable to those of the well-known pore-forming polypeptide gramicidin D (20 μg/mL) treated cells (Figure 10D). Overall, observations obtained with the help of TEM lend support to the calcein leakage assay that confirms membrane perturbation as the mode of action because of $[Mn^{II}(Cur)_2(HCur)]$.

https://dx.doi.org/10.1021/acsomega.9b04079
ACS Omega 2020, 5, 16342−16357

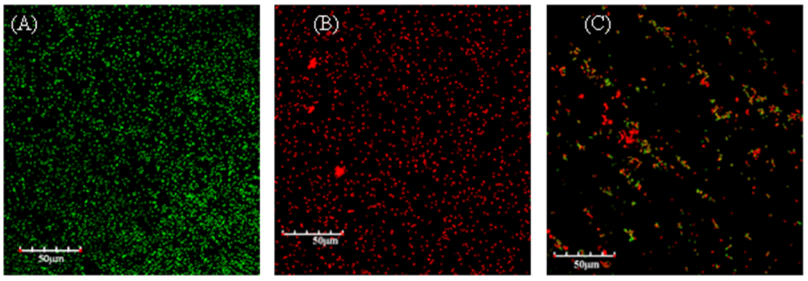

Figure 9. Fluorescence microscopy assay for viability of *S. aureus* ATCC 29213 treated with 50 μM HCur and $[Mn^{II}(Cur)_2(HCur)]$ for 2 h after staining with fluorescent probes SYTO 9 and PI. Representative merged image of both (FITC + PI) channels of (A) untreated control cells, (B) $[Mn^{II}(Cur)_2(HCur)]$, and (C) HCur. Green indicates live bacteria and red indicates dead and membrane-damaged bacterial cells.

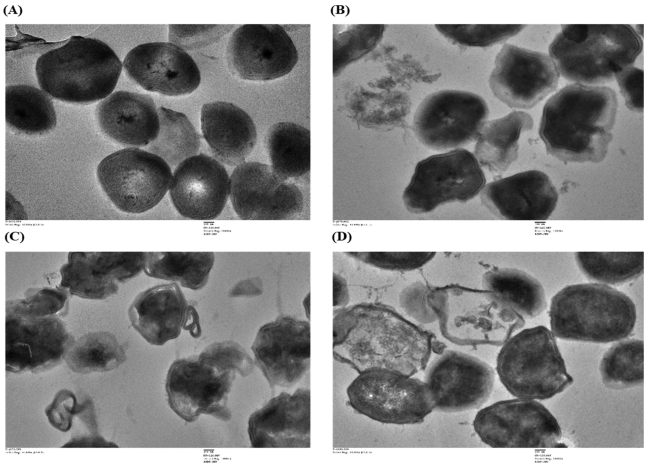

Figure 10. TEM images of *S. aureus* ATCC 29213 treated with 50 μM of HCur, $[Mn^{II}(Cur)_2(HCur)]$, and 20 μg/mL gramicidin D for 2 h. (A) Untreated control cells, (B) HCur, (C) $[Mn^{II}(Cur)_2(HCur)]$, and (D) gramicidin D-treated cells.

2.7.6. Comparative DNA Binding Ability of $[Mn^{II}(Cur)_2(HCur)]$. Although membrane permeabilization occurred within 2 min of incubation of $[Mn^{II}(Cur)_2(HCur)]$ (Figure 7A), no effective killing was observed in that time scale (Figure 6). This suggests that there might be some intracellular targets as well. To explore further on possible intracellular targets, the DNA-binding ability of $[Mn^{II}(Cur)_2(HCur)]$ was compared with HCur using the gel retardation assay or electrophoretic mobility shift assay, which is a common electrophoresis technique to study the affinity of test compounds toward DNA. Figure 11 shows evidence for binding of $[Mn^{II}(Cur)_2(HCur)]$ with DNA (100 ng) at 25 and 50 μM, respectively, reflected by retardation in electrophoretic mobility of plasmid DNA. When compared with $[Mn^{II}(Cur)_2(HCur)]$, HCur did not show effective DNA binding, that is, it did not retard the mobility of plasmid DNA under similar conditions (Figure 11). Indolicidin was used as the control for DNA-binding studies, showing that the concentration required was 12.5 μM. Such DNA-binding studies reveal a high affinity of $[Mn^{II}(Cur)_2(HCur)]$ for plasmid DNA against that observed with HCur, suggesting it to be the cause of intracellular plasmid DNA targeting that could be another mode for antibacterial activity due to $[Mn^{II}(Cur)_2(HCur)]$.

Based on the studies mentioned above, it could now be said that $[Mn^{II}(Cur)_2(HCur)]$ targets bacterial cell membranes as well as the DNA of *S. aureus*. There are several reports suggesting that membrane permeabilization alone is not

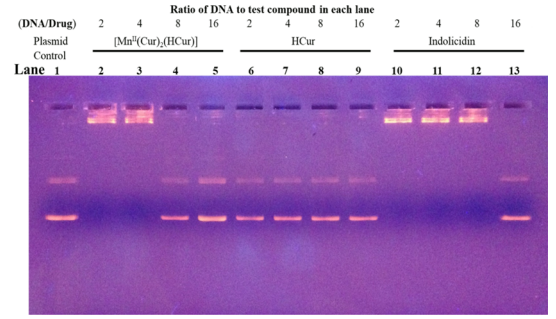

Figure 11. Plasmid DNA-binding ability of $[Mn^{II}(Cur)_2(HCur)]$, HCur, and indolicidin compared using 1.0% agarose gel electrophoresis. Lane 1 denotes plasmid DNA alone; lanes 2−5 denote plasmid DNA in the presence of 50, 25, 12.5, 6.25 μM $[Mn^{II}(Cur)_2(HCur)]$; lanes 6−9 denote plasmid DNA in the presence of 50, 25, 12.5, 6.25 μM HCur; lanes 10−13 denote plasmid DNA in the presence of 50, 25, 12.5, 6.25 μM indolicidin.

sufficient to kill bacterial cells and that intracellular targets such as DNA have an important role in bactericidal action.[53,54] In fact, our results with HCur and $[Mn^{II}(Cur)_2(HCur)]$ hint in that direction. We feel that the cytoplasmic membrane may not be the primary target and that there are probably roles of intracellular targets such as DNA as well, which get modified following interaction with compounds. Hence, a combination of both aspects could probably be the reason for the complex's potential staphylocidal action.

2.8. $[Mn^{II}(Cur)_2(HCur)]$ Was Nonhemolytic and Nontoxic toward Mammalian Cells. As HCur does not possess any toxicity, it becomes essential to know if following complex formation, any toxicity is developed in mammalian cells. Hence, the toxicity of $[Mn^{II}(Cur)_2(HCur)]$ was evaluated by studying its hemolytic and cytotoxic activity against mouse red blood cells (RBCs) and the 3T3 murine fibroblast cell line, respectively. For this purpose, much higher concentrations (250 and 500 μM) were used, which are well above the dose required for antibacterial activity. As evident from Figure 12A, similar to HCur, $[Mn^{II}(Cur)_2(HCur)]$ was nearly nonhemolytic. It was 2.60 ± 1.60% hemolytic at 250 μM and 9.68 ± 0.93% at 500 μM; 0.1% Triton X-100 was used as the positive control in the experiment.

To further rule out any potential toxicity, cytotoxicity of $[Mn^{II}(Cur)_2(HCur)]$ was also determined on the 3T3 murine fibroblast cell line using the 3-(4,5-dimethylthiazol-2-yl)-2,5-diphenyltetrazolium bromide (MTT) assay and the result was compared to that of HCur. As shown in Figure 12B, $[Mn^{II}(Cur)_2(HCur)]$ showed cytotoxicity of 6.74 ± 2.91% (at 250 μM) and 11.26 ± 5.02% (at 500 μM), which was in

https://dx.doi.org/10.1021/acsomega.9b04079
ACS Omega 2020, 5, 16342−16357

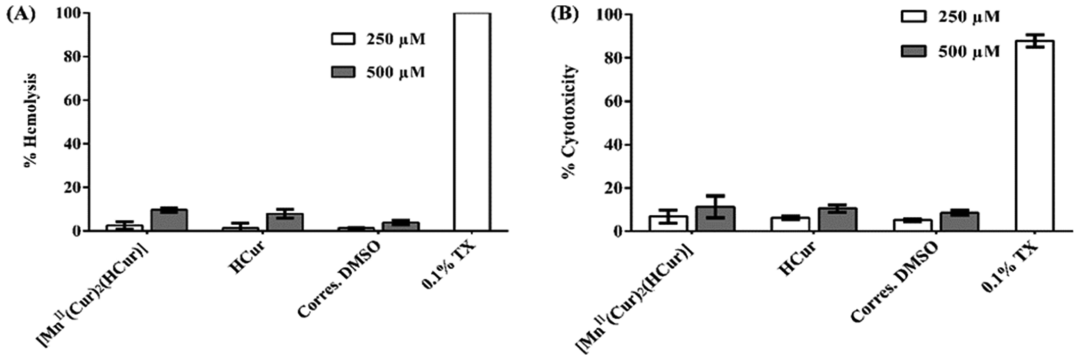

Figure 12. (A) Hemolytic activity of $[Mn^{II}(Cur)_2(HCur)]$ and HCur on mouse RBC. For the experiment, 0.1% Triton X-100 was used as the positive control (considering 100% hemolysis). The experiment was performed in duplicate on two different days; each data point represents mean ± SD; (B) cytotoxicity of $[Mn^{II}(Cur)_2(HCur)]$ and HCur on the 3T3 murine fibroblast cell line. Percentage viability of cells relative to the untreated control was measured using an MTT assay; % cytotoxicity is presented. The experiment was performed in triplicate on three different days; each data point represents mean ± SD.

the same range of toxicity observed for HCur. A 2.0% Triton X-100 was used as the positive control, showing 83.60 ± 5.38% cytotoxicity relative to an untreated growth as the control. Hence, altogether, it is evident that the studied complex exhibited little or no toxicity on mammalian RBCs and the fibroblast cell line even at concentrations much higher than one would use as a dose for antibacterial activity.

3. CONCLUSIONS

In the present study, a complex of Mn^{II} with curcumin $[Mn^{II}(Cur)_2(HCur)]$ was prepared and characterized. Although the reported complex did not show a significant improvement in aqueous solubility, it was however found to be stable in different biological milieu as compared to HCur. The complex showed a significant enhancement in antibacterial activity against clinically relevant pathogens like *S. aureus* and *E. coli* when compared with HCur. The complex first binds to LPSs of the outer leaflet of the outer membrane of *E. coli*. This binding probably leads to disruption of the outer membrane, which then induces permeabilization in the cytoplasmic membrane of bacteria as evident from the LPS-binding assay. For *S. aureus*, the calcein leakage assay clearly established the bacterial membrane disruption by the complex. This membrane-targeting mode of action was further corroborated by SEM and TEM techniques, showing remarkable morphological changes on the *S. aureus* cell surface. Apart from membrane disruption, it also targets intracellular DNA as it shows reasonably good binding for DNA, as evident from the gel retardation assay using bacterial plasmid DNA. The complex showed a significant SOD-like activity leading to generation of ROS, which might contribute toward bacterial cell killing. H_2O_2 formed as a consequence probably interacts with bacterial cells showing enhanced antibacterial activity compared to HCur. The metal ion in the complex being Mn^{II}, capable of reaching a higher oxidation state in the presence of peroxide might also show oxidative stress.[55] The multitargeting mode of activity of the complex not only boosts its antibacterial potency but also makes it difficult for bacteria to generate a resistance against it. Moreover, $[Mn^{II}(Cur)_2(HCur)]$ showed almost no detrimental effect on mammalian cells. Therefore, the complex could become an excellent candidate for therapeutic use. The study provides valuable information for further research for a therapeutic application of the complex at a time of increasing resistance to almost all conventional antibiotics.

4. EXPERIMENTAL SECTION

4.1. Materials. HCur was purchased from Sigma-Aldrich and carefully stored at −5 °C. Stock solutions were prepared in ethanol/DMSO before an experiment and if required stored in the dark. $MnCl_2{\cdot}4H_2O$ was purchased from E. Merck, India. Phosphate buffer was prepared in Millipore water. Sodium nitrate (AR) was used to maintain the ionic strength of the medium. Calf thymus DNA purchased from Sisco Research Laboratories, India, was dissolved in Millipore water containing 120 mM NaCl, 35 mM KCl, and 5 mM $CaCl_2$. Absorbance of the DNA solution was recorded at 260 and 280 nm, respectively, and A_{260}/A_{280} was noted. The ratio found in the range 1.8−1.9 suggests the DNA to be sufficiently free from protein, requiring no further purification. The DNA was also characterized by measuring its circular dichroism (CD) spectra at 260 nm on a CD spectropolarimeter (J815, JASCO, Japan). Plasmid DNA was purchased from Agilent Technologies and used without further purification. The concentration of DNA was determined in terms of nucleotide, considering the molar extinction coefficient at 260 nm to be 6600 M^{-1} cm^{-1}. Nitroblue tetrazolium dichloride (NBT^{2+}), MTT, calcein-acetoxy methyl ester (calcein-AM), LPS *E. coli* (055:B5), and gramicidin D were purchased from Sigma-Aldrich. LIVE/DEAD BacLight Bacterial Viability Kit (L7007) and BODIPY-TR-cadaverine dye were procured from Invitrogen. Agar powder, Luria-Bertani (LB) broth, and Brain Heart Infusion (BHI) medium were purchased from HiMedia Laboratories. Mueller−Hinton broth (MHB) and Dulbecco's modified Eagle's medium (DMEM) were procured from Difco and HiMedia, respectively

4.1.1. Bacterial Strain Used. *S. aureus* (ATCC 29213) and *E. coli* (ATCC 25922) were used in the study. Bacterial strains were stored as frozen stock in 15% (v/v) glycerol at −80 °C till subcultured at 37 °C on BHI and LB agar plates for further studies.

4.2. Methods. *4.2.1. Determination of pK_a of Curcumin.* Dissociation of protons on HCur was determined with the help of pH-metric titrations (eqs S1 and S2) carried out in ethanol (10%)−aqueous (90%) solution at 32 °C and an ionic strength due to 0.1 M $NaNO_3$. pH was recorded using a pH meter (Equip-Tronics EQ-610, India); pH values were suitably

https://dx.doi.org/10.1021/acsomega.9b04079
ACS Omega 2020, 5, 16342−16357

corrected and reported as would be in a pure aqueous solution. Change in absorbance of HCur was followed at 467 nm. Dissociation of protons on HCur was evaluated using eq S3, Supporting Information. pK_{a1} = 7.17 ± 0.31; pK_{a2} = 10.5 ± 0.16; pK_{a3} = 11.44 ± 0.17 [Figure S13, Supporting Information]. Our values were in accordance with those determined earlier.[56−58]

4.2.2. Determination of Stoichiometry of Complex Formation between Mn^{II} and HCur by the Mole Ratio and Job's Method of Continuous Variation. The stoichiometry of complex formation was ascertained by mixing different volumes of equimolar Mn^{II} and HCur.[59,60] In the mole ratio method, in one set of experiments, the concentration of HCur was maintained constant and the concentration of Mn^{II} was varied, whereas in another, the concentration of Mn^{II} was constant and that of HCur was varied.[59,60] The absorbance recorded at 430 nm was plotted against $(T_M/T_L)_{TL}$ and $(T_L/T_M)_{TM}$ (Figure S14A,B). T_M and T_L are the concentrations of Mn^{II} and HCur in experimental solutions, respectively. Straight lines were obtained, the intersection of which indicates the ratio in which HCur binds to Mn^{II}. In Job's method of continuous variation (Figure S14C), absorbance was recorded at 430 nm and plotted against volumes of HCur and Mn^{II}.[59,60] The stoichiometry of Mn^{II} to HCur was found in the range 1:2 to 1:3, gradually tending to 1:3.

4.2.3. Determination of pK_a of HCur in the Presence of Mn^{II}. Dissociation of a proton of HCur in the presence of Mn^{II} was determined in ethanol (10%)−aqueous (90%) solution at 32 °C and a fixed ionic strength of the medium because of 0.1 M $NaNO_3$. Absorbance of HCur was followed at 430 nm in the presence of Mn^{II} and fitted to eq S4, Supporting Information. pK_{a1} (=5.89 ± 0.43) and pK_{a2} (=8.83 ± 0.20) were determined (Figure S15, Supporting Information). Titration data were also fitted to eq S3, Supporting Information, able to determine dissociations of three protons. However, when the data were fitted to eq S3, Supporting Information values for pK_{a1} and pK_{a2} remained the same as that obtained from eq S4, Supporting Information, but the value for pK_{a3} was 12.44 ± 23.07, which is absurd. Hence, we concluded that in the presence of Mn^{II}, the two phenolic −OH protons present on HCur dissociate simultaneously as determined from eq S3, Supporting Information. Stability constants β^* and β were determined using eqs S5−S9, Supporting Information, and found to be 2.52×10^{18} ($\log \beta$ = 18.4).

4.2.4. Preparation of the Complex. HCur (0.2762 g, 0.75 mmol) was dissolved in 15 mL of deaerated acetonitrile−ethanol mixture (1:3). The solution was neutralized with triethylamine (0.104 mL, 0.75 mmol), followed by the addition of $MnCl_2 \cdot 4H_2O$ (0.0495 g, 0.25 mmol) dissolved in 10 mL of deaerated ethanol−water mixture (1:1). Argon was passed through the mixture to maintain an inert atmosphere. The whole setup was stirred for 24 h. A greenish brown precipitate was recovered and washed with chloroform, diethyl ether, ethanol, tetrahydrofuran, and acetonitrile separately depending on the solubility of HCur in these solvents to wash away undesired impurities. A pure complex was obtained. Percentage yield: ∼60%. Elemental analysis was done on a PerkinElmer 2400 Series-II CHN analyzer. Anal. Calcd (%) for $C_{63}H_{58}O_{18}Mn$: C, 65.32; H, 5.052. Found: C, 65.12; H, 5.16. The complex was not soluble in common solvents such as methanol, ethanol, acetonitrile, dichloromethane. It was soluble partly in dimethyl formamide and reasonably well in DMSO.

4.2.5. DFT Calculations. DFT is an important tool to study the geometry, electronic structure, and optical properties of a compound. It is very useful in situations where the structure of the compound cannot be obtained experimentally. In such cases, an attempt for a structure is made with the help of DFT calculations that are performed based on experimental (e.g., spectroscopic) evidence. The TD-DFT approach has also been demonstrated to be reliable for calculating spectral properties of many transition-metal complexes.[61] In our case, in the absence of a crystal structure, we optimized the molecular geometry of HCur and the complex formed with Mn^{II} by DFT using the Gaussian 09 package.[62] The ligand (HCur) geometry was optimized with Becke3 parameter hybrid exchange functional and Lee−Yang−Parr correlation functional (B3LYP)[63] with the 6-31+G(d,p) basis set. Optimization of the complex was done using unrestricted hybrid DFT by Becke's three-parameter exchange functional[63,64] with the nonlocal Lee−Yang−Parr electron correlation functional (UB3LYP model).[63,64] The basis set chosen for Mn was LANL2DZ (ECP)[65] and this was used jointly with the 6-31G(d,p) basis set for other atoms, namely, C, H, and O, using Gaussian 09.[62] TD-DFT was performed considering optimized geometry using the CAM-B3LYP[63,66,67] function in combination with LANL2DZ (ECP) for the Mn atom[65] and 6-31G(d,p) for other atoms (C, H, and O) to calculate spectral properties of the complex. The geometry of the ligand and the complex was fully optimized without any symmetry constraints. The Gauss Sum 2.1 program[68] was used for calculating molecular orbital contributions from atoms or groups.

4.2.6. Comparative Analysis of Stability of HCur and the Complex in Physiological Buffer and Various Cell Media. To evaluate the stability of HCur and $[Mn^{II}(Cur)_2(HCur)]$ under physiological buffer conditions (PBS pH = 7.4) and in different bacterial growth media [BHI, MHB, and Dulbecco's modified Eagle's medium (DMEM)], absorption spectra were recorded with the help of a UV−vis spectrophotometer. HCur and the complex were dissolved in DMSO. From a stock of concentration 20 mM, 1 μL was taken and added to 1 mL of PBS buffer (10 mM sodium phosphate, 150 mM NaCl, pH 7.4) or to 1 mL of growth medium to achieve a final concentration of 25 μM. The absorption spectrum of the mixture was recorded for 20 min at an interval of 5 min. As the environment of most cellular compartments is reducing in nature, we investigated the stability of HCur and $[Mn^{II}(Cur)_2(HCur)]$ in the presence of 10 μM DTT, a strong reducing agent.[32] DTT is one of the most commonly used reducing agents in biological buffers, and previous reports suggest that HCur loses its biological activity when treated with DTT as it accelerates degradation of HCur.[69]

4.2.7. Interaction of $[Mn^{II}(Cur)_2(HCur)]$ with Calf Thymus DNA. As HCur dissolved in phosphate buffer (pH = 7.4) is prone to changes, realized from a change in absorbance, DNA-binding studies using UV−vis spectroscopy were not attempted. However, titration of the complex was carried out as it did not show any appreciable change in absorbance in the same medium (pH 7.4) when followed for a certain length of time. In case of the complex, a change in absorbance of the solution observed upon addition of calf thymus DNA could then be attributed to an interaction of the complex with DNA. This was followed on a JASCO V-630 spectrophotometer and analyzed according to eqs 1−6.

https://dx.doi.org/10.1021/acsomega.9b04079
ACS Omega 2020, 5, 16342−16357

$$L + DNA \rightleftharpoons L - DNA \qquad K_d = \frac{[L][DNA]}{[L - DNA]} \tag{1}$$

L represents the complex and K_d the dissociation constant whose reciprocal provides a value for the apparent binding constant (K_{app}).[33,36−39] Equation 2 is generated from eq 1 where the reciprocal of the change in absorbance was plotted against the reciprocal of ($C_D - C_0$). C_D refers to concentration of calf thymus DNA and C_0 to complex. Using eq 2, ΔA_{max} and K_{app} ($=K_d^{-1}$) may be determined from the intercept and slope, respectively.

$$\frac{1}{\Delta A} = \frac{1}{\Delta A_{max}} + \frac{K_d}{\Delta A_{max}(C_D - C_0)} \tag{2}$$

ΔA denotes the change in absorbance of the complex at a definite pH at which binding experiments were done. For each titration curve, ΔA_{max} indicates the maximum change in absorbance.

$$K_d = \frac{\left[C_0 - \left(\frac{\Delta A}{\Delta A_{max}}\right)C_0\right]\left[C_D - \left(\frac{\Delta A}{\Delta A_{max}}\right)C_0\right]}{\left(\frac{\Delta A}{\Delta A_{max}}\right)C_0} \tag{3}$$

$$C_0\left(\frac{\Delta A}{\Delta A_{max}}\right)^2 - (C_0 + C_D + K_d)\left(\frac{\Delta A}{\Delta A_{max}}\right) + C_D = 0 \tag{4}$$

Equations 3 and 4 were used to fit the data by nonlinear square fit analysis and eq 5 to another form of a double reciprocal plot that has an intercept on y-axis = 1, providing values for apparent binding constants.[33,36−39] The plot of $\Delta A/\Delta A_{max}$ versus ratio of the concentration of calf thymus DNA to the complex provides two straight lines whose intersection gives us n_b, the site size of interaction, indicating the number of nucleotides bound to the complex. Apparent binding constants, when multiplied with n_b, provide the overall binding constant (K').

$$\frac{1}{(C_b/C_L)} = 1 + \frac{1}{[K][C_D]} \tag{5}$$

The titration data were also analyzed by a modified form of the original Scatchard equation [eq 6] and the overall binding constant (K') and site size ($n = n_b^{-1}$) were determined.[40]

$$r/C_f = K'(n - r) \tag{6}$$

$r = C_b/C_D$; C_b is the concentration of the bound form of the complex and C_f, the free form. "n" provides binding stoichiometry in terms of bound complex per nucleotide and is the reciprocal of "n_b".

4.2.8. SOD Activity of the Complex. Superoxide was generated by an enzyme assay using hypoxanthine/xanthine oxidase with some modifications of a method described earlier.[70,71] The reactions involved are mentioned below

$$\text{hypoxanthine} + H_2O + O_2 \rightarrow \text{xanthine} + H_2O_2 \tag{7}$$

$$\text{xanthine} + H_2O + O_2 \rightarrow \text{uric acid} + H_2O_2 \tag{8}$$

$$\text{xanthine} + H_2O + 2O_2 \rightarrow \text{uric acid} + 2O_2^- + 2H^+ \tag{9}$$

A mixture of 50 μM hypoxanthine, 300 μM NBT^{2+}, 0.04 unit/mL xanthine oxidase, and 0−50 μM $[Mn^{II}(Cur)_2(HCur)]$ dissolved in 10% DMSO and 20 mM phosphate buffer (pH 7.4) was incubated at 25 °C for 10 min. The NBT^+ formed was measured using a spectrophotometer at 524 nm. Percentage inhibition of NBT^+ formation was calculated using eq 10.

$$\%\ \text{inhibition} = (A_0 - A_s) \times 100/A_0 \tag{10}$$

A_0 and A_s are the absorbance because of NBT^+ at 524 nm in the absence and presence of $[Mn^{II}(Cur)_2(HCur)]$, respectively. Percentage inhibition was plotted as a function of $[Mn^{II}(Cur)_2(HCur)]$. Similar experiments were repeated with the native SOD enzyme. Percentage inhibition due to $[Mn^{II}(Cur)_2(HCur)]$ was compared to SOD recorded under identical conditions.

4.2.9. Killing Assay. The killing assay was performed according to procedures mentioned in the literature.[12,72] Bacterial cells were grown in BHI broth to a mid-logarithmic phase. Cells were then centrifuged, washed, and resuspended in PBS buffer (10 mM sodium phosphate, 150 mM NaCl, pH 7.4). Resuspended cells were adjusted to an OD_{600} of 0.5 spectrophotometrically (~10^8 cfu/mL). A final inoculum of 10^5 cfu/mL was exposed to various concentrations of $[Mn^{II}(Cur)_2(HCur)]$ and HCur in PBS buffer. At selected time points (2, 60, and 120 min), aliquots were plated on a BHI agar plate in triplicate and incubated overnight at 37 °C. Bacterial colonies were counted the following day and bacterial survival expressed as mean percentage versus nontreated control (set as 100% survival). Each experiment was repeated independently on three separate days.

4.2.10. Bacterial Membrane Permeabilization Assay. Bacterial membrane permeabilization due to $[Mn^{II}(Cur)_2(HCur)]$ and HCur exposure was quantified by calcein leakage assay using flow cytometry, as described earlier.[12,49,74] Calcein-AM is a membrane-permeating, nonfluorescent derivative of calcein. After entering cells, calcein-AM is cleaved by cytoplasmic esterases, releasing fluorescent calcein, which is membrane-impermeable. Therefore, calcein can leak out of cells only if the membrane is damaged. Briefly, *S. aureus* ATCC 29213 cells were grown to mid-logarithmic phase in BHI medium and adjusted to OD_{600} of 1.0 (~10^9 cfu/mL) in PBS buffer as previously mentioned. Mid-log cells (10^8 cfu/mL) were loaded with 2 μg/mL of calcein-AM by incubating them in the dark at 37 °C for 2 h. Calcein-loaded cells were diluted to 10^6 cfu/mL and treated with 25 or 50 μM $[Mn^{II}(Cur)_2(HCur)]$ and HCur for 2 h at 37 °C. Afterward, the fluorescence of cell-entrapped calcein was quantified using a flow cytometer (BD FACSVerse, San Jose, CA) with excitation and emission wavelengths of 490 and 517 nm, respectively. A total of 10,000 cells were acquired for each flow cytometer analysis. Cells showing <10 fluorescence units (FL units) were inferred to have lost calcein because of drug-induced permeabilization and cells showing >10 FL units were interpreted to have retained calcein, indicative of an intact membrane. Untreated calcein-loaded cells were considered as the negative control and 20 μg/mL gramicidin D, a well-known pore-forming antimicrobial peptide-treated cells as the positive control. Release of calcein from treated samples was measured on three different days.

4.2.11. LPS-Binding Assay. The binding affinity of the complex to LPS was quantified by a fluorescence-based displacement assay using BODIPY-TR-cadaverine, as previously described.[51] Fluorescence of this dye is quenched upon binding to LPS, and displacement of the dye by the test

https://dx.doi.org/10.1021/acsomega.9b04079
ACS Omega 2020, 5, 16342−16357

compound results in dequenching of BODIPY-TR-cadaverine fluorescence. For this displacement assay, a stock solution of BODIPY-TR-cadaverine and LPS was diluted in 50 mM Tris buffer (pH 7.4) to yield a final concentration of 5 μg/mL BODIPY-TR-cadaverine and 50 μg/mL of LPS. The background fluorescence of this mixture was recorded with SpectraMax iD5 Multi-Mode Microplate Reader (excitation wavelength was 580 nm; emission wavelength was 620 nm). The change in fluorescence with different concentrations of the complex and HCur was recorded up to 30 min.

4.2.12. Fluorescence Microscopy. Bacterial viability was analyzed using a LIVE/DEAD BacLight Bacterial Viability Kit according to the manufacturer's protocol. Briefly, a dye mixture was prepared containing an equal volume of SYTO 9 and PI.[12,52] The bacterial suspension (10^9 cfu/mL) treated with 50 μM HCur and $[Mn^{II}(Cur)_2(HCur)]$ for 2 h was incubated with 3 μL of dye mixture for each milliliter of bacterial suspension for 15 min in the dark. A 5 μL aliquot of the stained bacterial suspension was trapped between a glass slide and a coverslip. The slide was observed under a confocal fluorescence microscope (Olympus Fluoview FV 1000) using 60× objective with FITC (corresponding to SYTO 9) and PI filters. The excitation/emission maxima were 480/500 nm for SYTO 9 and 490/635 nm for PI, respectively.

4.2.13. Scanning Electron Microscopy. Bacterial samples for SEM measurements were prepared as described earlier.[12,52] Briefly, mid-logarithmic phase cells of *S. aureus* ATCC 29213 (10^9 cfu/mL) were treated with 50 μM HCur and $[Mn^{II}(Cur)_2(HCur)]$ for 2 h at 37 °C with shaking. Gramicidin D (20 μg/mL)-treated cells and untreated bacterial cells were used as the control. After incubation, the cells were washed thrice with 10 mM phosphate buffer (NaH_2PO_4/Na_2HPO_4, pH 7.4) and then fixed with 2.5% glutaraldehyde overnight at 4 °C. The following day, the cells were again washed thrice with the same buffer and dehydrated sequentially with 30−100% ethanol for 10 min each. They were then dried on a coverslip under vacuum in a desiccator. Finally, the cells were coated with gold and viewed via a scanning electron microscope (EVO 40, Carl Zeiss, Germany) available at AIRF, JNU. The experiment was performed twice independently on two separate days. Similar images were obtained.

4.2.14. Transmission Electron Microscopy. For TEM, bacterial samples were prepared according to a protocol described earlier.[12,52] Samples were prepared as described for SEM until overnight fixation with 2.5% glutaraldehyde at 4 °C. Further, 1% osmium tetroxide was used to postfix cells and then sequentially dehydrated by 50−100% acetone. Each sample was embedded in epoxy resin, and ultrathin sections were prepared using a microtome. The sections were placed on a copper grid and stained with uranyl acetate, followed by lead citrate. The samples were then washed twice in Milli-Q water and dried under vacuum in a desiccator. The grid was viewed via a transmission electron microscope (Zeol-JEM 2100, Japan) available at AIRF, JNU.

4.2.15. DNA Gel Retardation Assay. Shift in mobility of plasmid DNA upon interaction with HCur and $[Mn^{II}(Cur)_2(HCur)]$ was determined using a gel retardation assay, which is a common electrophoresis technique used to study the interaction of a test compound with DNA. This experiment was performed using a protocol described earlier.[49] In brief, 100 ng of plasmid DNA was incubated with different concentrations of $[Mn^{II}(Cur)_2(HCur)]$ and HCur for 1 h at room temperature in binding buffer (5% glycerol, 10 mM Tris-HCl (pH 8.0), 1 mM ethylenediaminetetraacetic acid (EDTA), 1 mM DTT, 20 mM KCl, and 50 μg/mL bovine serum albumin). Afterward, 4 μL of a native loading buffer (10% Ficoll 400, 10 mM Tris-HCl, pH 7.5, 50 mM EDTA, 0.25% bromophenol blue, and 0.25% xylene cyanol) was added. The reaction mixture was loaded onto 1% agarose gel with ethidium bromide using 0.5 times Tris borate−EDTA buffer (45 mM Tris-borate and 1 mM EDTA, pH 8.0). In this assay, a well-known DNA-binding peptide indolicidin was used as control.[73] The experiment was repeated on three different days. Similar results were obtained.

4.2.16. Hemolytic Assay. The ability of $[Mn^{II}(Cur)_2(HCur)]$ and HCur to induce hemolysis was assessed according to a protocol described earlier.[50,74] Briefly, fresh mice blood was collected and centrifuged at 1500 rpm for 10 min to remove blood plasma. The pellets of RBCs were washed thrice in 35 mM PBS buffer and resuspended in 4% v/v of the same buffer. In a 96-well plate, the compounds were serially diluted to a final volume of 100 μL in each well. Next, 100 μL of RBC suspension was added to each well and incubated at 37 °C for 1 h. The accompanying DMSO used to dissolve $[Mn^{II}(Cur)_2(HCur)]$ was also tested under identical conditions. After incubation, the plates were centrifuged at 1500 rpm for 10 min. The supernatant (20 μL) was added to 80 μL of PBS in a fresh 96-well plate. Hemoglobin release was measured at 414 nm using a Thermo Scientific Varioskan Flash Multiplate reader. For positive control, 0.1% Triton X-100 was used, and for negative control, RBC in PBS buffer was used. Percentage hemolysis was determined using eq 11.

$$\%\ \text{hemolysis} = [(\text{OD of sample} - \text{OD of PBS}) / (\text{OD of 0.1\% Triton X} - \text{OD of PBS})] \times 100 \quad (11)$$

The experiment was performed in accordance with the guidelines of CPCSEA (Committee for the Purpose of Control and Supervision of Experiments on Animals) and Institutional Animal Ethics Committee (IAEC-23/2018) of Jawaharlal Nehru University, New Delhi, India.

4.2.17. Cytotoxicity Assay. The cytotoxicities of HCur and $[Mn^{II}(Cur)_2(HCur)]$ on mouse fibroblast 3T3 cells were determined by an MTT assay.[50,74] Briefly, 3T3 cells were seeded in DMEM supplemented with 10% fetal bovine serum (FBS) and antibiotics (1× anti−anti) until they reached over 75% confluency. Cells were added to each well of a 24-well plate to a final count of 0.2×10^5 cells/well and incubated for 24 h at 37 °C in a 5% CO_2 incubator. After 24 h, the medium was removed. The cells were suspended in fresh media with 10% FBS and treated with 250 and 500 μM each of HCur and $[Mn^{II}(Cur)_2(HCur)]$ that were dissolved in DMSO. The final DMSO concentration in the reaction mixture was less than 0.5%. The DMSO concentration accompanying the compounds was tested under similar conditions. After 4 h of incubation in a 5% CO_2 atmosphere, the medium was carefully aspirated, and 1 mL of the MTT solution (0.1 mg/mL) was added to each well. The plate was incubated for 2 h at 37 °C in the dark in a 5% CO_2 atmosphere. Later, the plate was centrifuged at 1000 rpm for 5 min, and the supernatant was removed. Subsequently, 100 μL of DMSO was added to solubilize the formazan crystals formed by reduction of the tetrazolium salt. OD was measured at 570 nm, and the

https://dx.doi.org/10.1021/acsomega.9b04079
ACS Omega 2020, 5, 16342−16357

percentage survival was determined using eq 12. The assay was repeated on three separate days.

$$\text{Cell viability (\%)} = [(\text{OD}_{570} \text{ of sample}) / (\text{OD}_{570} \text{ of untreated control})] \times 100 \quad (12)$$

■ ASSOCIATED CONTENT

Supporting Information

The Supporting Information is available free of charge at https://pubs.acs.org/doi/10.1021/acsomega.9b04079.

Absorption spectra of curcumin and the Mn^{II} complex in DMSO; absorption spectra of Mn^{II} interacting with curcumin during determination of stoichiometry of complex formation; IR spectrum of curcumin; IR spectrum of $[Mn^{II}(Cur)_2(HCur)]$; TGA of $[Mn^{II}(Cur)_2(HCur)]$; keto−enol tautomerism of curcumin; optimized bond lengths for carbon−oxygen bonds of curcumin involved in coordination of Mn^{II}; behavior of curcumin and its Mn^{II} complex realized from a change in absorbance on being taken in PBS buffer or in PBS buffer with 10 μM DTT; behavior of curcumin and the Mn^{II} complex realized from a change in absorbance when taken in different bacterial growth mediums; double reciprocal plot for interaction of $[Mn^{II}(Cur)_2(HCur)]$ with calf thymus DNA; double reciprocal plot with y intercept = 1 for interaction of $[Mn^{II}(Cur)_2(HCur)]$ with calf thymus DNA; bacterial survival in logarithmic scale, indicating the antibacterial efficacy of $[Mn^{II}(Cur)_2(HCur)]$ and curcumin on *S. aureus* and *E. coli* cells; SEM images of *S. aureus* ATCC 29213 treated with either no compound or with curcumin, $[Mn^{II}(Cur)_2(HCur)]$, and gramicidin D to realize membrane permeabilization by the calcein leakage assay; equations related to dissociation of the three protons on curcumin; spectrophotometric titration of curcumin; mole ratio and Job's plots of continuous variation for curcumin with Mn^{II}; spectrophotometric titration of curcumin in the presence of Mn^{II}; and evaluation of the stability constant of the complex formed in solution (PDF)

■ AUTHOR INFORMATION

Corresponding Authors

Saurabh Das − *Department of Chemistry, Jadavpur University, Kolkata 700032, India;* orcid.org/0000-0002-0455-8760; Phone: +91 33 24572148; Email: dasrsv@yahoo.in; Fax: +91 33 24146223

Kasturi Mukhopadhyay − *School of Environmental Sciences, Jawaharlal Nehru University, New Delhi 110067, India;* orcid.org/0000-0002-6886-1080; Email: kasturim@mail.jnu.ac.in, kasturi26@hotmail.com

Authors

Tanmoy Saha − *Department of Chemistry, Jadavpur University, Kolkata 700032, India*

Prince Kumar − *School of Environmental Sciences, Jawaharlal Nehru University, New Delhi 110067, India;* orcid.org/0000-0002-8326-1382

Nayim Sepay − *Department of Chemistry, Jadavpur University, Kolkata 700032, India;* orcid.org/0000-0001-7702-3989

Durba Ganguly − *Department of Inorganic Chemistry, Indian Association for the Cultivation of Science, Kolkata 700032, India*

Kanchan Tiwari − *School of Environmental Sciences, Jawaharlal Nehru University, New Delhi 110067, India*

Complete contact information is available at: https://pubs.acs.org/10.1021/acsomega.9b04079

Author Contributions

‖T.S. and P.K. have equal contributions.

Notes

The authors declare no competing financial interest.

■ ACKNOWLEDGMENTS

P.K. and K.T. acknowledge UGC for an SRF and a non-NET fellowship, respectively. T.S. is grateful to the "Governing body" of Sri Aurobindo Institute of Education, Salt Lake, Kolkata for permission to pursue research leading to a Ph D degree. S.D. wishes to thank the RUSA 2.0 program of the Government of India, operating at Jadavpur University under which he received a "Research Support to Faculty Members" in the Research Thrust Area "Research in Sustainable Development", Sanction ref. no. R-11/438/19 dated 30.05.2019. Besides, S.D. is grateful to the DST-PURSE program of the Government of India for financial support to the Department of Chemistry, Jadavpur University, from where funds were used for this study (for purchase of chemicals). He acknowledges the support received from UGC, New Delhi, through funding of the research program on "Advanced Materials" as part of UPE II to Jadavpur University and also acknowledges the UGC-CAS II program operating at the Department of Chemistry, Jadavpur University, for financial support to purchase "Chemicals and Glassware". This work was also supported by financial grants to K.M. from DST-SERB (EMR/2016/001708) and DBT (BT/PR27737/MED/29/1265/2018). K.M. is also grateful for receiving funds from DST-PURSE (Phase-II) and UGC (UPE-II: ID 59), which came to Jawaharlal Nehru University. The authors wish to thank Dr. Partha Ray, Department of Chemistry, JU, for kindly providing the IR data of the complex, Dr. Shouvik Chattopadhyay, Department of Chemistry, JU, for some useful discussions on the structure of the complex, Ashok Sahu, Dr. Ruchita Pal, and Manu Vashistha, AIRF, JNU, for their help in acquisition of confocal microscopy, SEM, and TEM images, respectively. The authors are grateful to the three reviewers who reviewed the manuscript with extreme care and provided suggestions for its improvement.

■ ABBREVIATIONS

HCur, curcumin; Cur^-, monoanionic Curcumin; *S. aureus*, *Staphylococcus aureus*; *E. coli*, *Escherichia coli*

■ REFERENCES

(1) Aggarwal, B. B.; Sundaram, C.; Malani, N.; Ichikawa, H. Curcumin: the Indian solid gold. *The molecular Targets and Therapeutic Uses of Curcumin in Health and Disease*; Springer, Boston, MA, 2007; pp 1−75.

(2) Jurenka, J. S. Anti-inflammatory properties of curcumin, a major constituent of *Curcuma longa*: a review of preclinical and clinical research. *Altern. Med. Rev.* **2009**, *14*, 141−153.

(3) Ak, T.; Gülçin, İ. Antioxidant and radical scavenging properties of curcumin. *Chem.-Biol. Interact.* **2008**, *174*, 27−37.

(4) Prasad, S.; Aggarwal, B. B. Turmeric, the Golden Spice, From Traditional Medicine to Modern Medicine. In *Herbal Medicine: Biomolecular and Clinical Aspects*, 2nd ed.; Benzie, I. F. F., Wachtel-Galor, S., Eds.; CRC Press/Taylor & Francis: Boca Raton (FL), USA, 2011; Chapter 13.
(5) Sato, H.; Chuang, V. T. G.; Yamasaki, K.; Yamaotsu, N.; Watanabe, H.; Nagumo, K.; Anraku, M.; Kadowaki, D.; Ishima, Y.; Hirono, S.; Otagiri, M.; Maruyama, T. Differential effects of methoxy group on the interaction of curcuminoids with two major ligand binding sites of human serum albumin. *PLoS One* **2014**, *9*, No. e87919.
(6) Wilken, R.; Veena, M. S.; Wang, M. B.; Srivatsan, E. S. Curcumin: A review of anti-cancer properties and therapeutic activity in head and neck squamous cell carcinoma. *Mol. Cancer* **2011**, *10*, 12.
(7) Wanninger, S.; Lorenz, V.; Subhan, A.; Edelmann, F. T. Metal complexes of curcumin - synthetic strategies, structures and medicinal applications. *Chem. Soc. Rev.* **2015**, *44*, 4986−5002.
(8) Teow, S.-Y.; Liew, K.; Ali, S. A.; Khoo, A. S.-B.; Peh, S.-C. Antibacterial action of curcumin against *Staphylococcus aureus*: A Brief Review. *J. Trop. Med.* **2016**, *2016*, 1−10.
(9) Bicer, N.; Yildiz, E.; Yegani, A. A.; Aksu, F. Synthesis of curcumin complexes with iron(III) and manganese(II), and effects of curcumin-iron(III) on Alzheimer's disease. *New J. Chem.* **2018**, *42*, 8098−8104.
(10) Goel, A.; Kunnumakkara, A. B.; Aggarwal, B. B. Curcumin as "Curecumin": From kitchen to clinic. *Biochem. Pharmacol.* **2008**, *75*, 787−809.
(11) Neelofar, K.; Shreaz, S.; Rimple, B.; Muralidhar, S.; Nikhat, M.; Khan, L. A. Curcumin as a promising anticandidal of clinical interest. *Can. J. Microbiol.* **2011**, *57*, 204−210.
(12) Tyagi, P.; Singh, M.; Kumari, H.; Kumari, A.; Mukhopadhyay, K. Bactericidal activity of curcumin I is associated with damaging of bacterial membrane. *PLoS One* **2015**, *10*, No. e0121313.
(13) Sharma, R. A.; Steward, W. P.; Gescher, A. J. Pharmacokinetics and pharmacodynamics of curcumin. *Adv. Exp. Med. Biol.* **2007**, *595*, 453−470.
(14) Banerjee, S.; Prasad, P.; Hussain, A.; Khan, I.; Kondaiah, P.; Chakravarty, A. R. Remarkable photocytotoxicity of curcumin in HeLa cells in visible light and arresting its degradation on oxovanadium (IV) complex formation. *Chem. Commun.* **2012**, *48*, 7702−7704.
(15) Mitra, K.; Gautam, S.; Kondaiah, P.; Chakravarty, A. R. Platinum(II) Complexes of Curcumin Showing Photocytotoxicity in Visible Light. *Eur. J. Inorg. Chem.* **2017**, 1753−1763.
(16) Banerjee, S.; Prasad, P.; Khan, I.; Hussain, A.; Kondaiah, P.; Chakravarty, A. R. Mitochondria targeting Photocytotoxic Oxidovanadium(IV) Complexes of Curcumin and (Acridinyl)-dipyridophenazine in Visible Light. *Z. Anorg. Allg. Chem.* **2014**, *640*, 1195−1204.
(17) Wang, Y.-J.; Pan, M.-H.; Cheng, A.-L.; Lin, L.-I.; Ho, Y.-S.; Hsieh, C.-Y.; Lin, J.-K. Stability of curcumin in buffer solutions and characterization of its degradation products. *J. Pharm. Biomed. Anal.* **1997**, *15*, 1867−1876.
(18) Kharat, M.; Du, Z.; Zhang, G.; McClements, D. J. Physical and chemical stability of curcumin in aqueous solutions and emulsions: Impact of pH, temperature, and molecular environment. *J. Agric. Food Chem.* **2017**, *65*, 1525−1532.
(19) Refat, M. S. Synthesis and characterization of ligational behavior of curcumin drug towards some transition metal ions: chelation effect on their thermal stability and biological activity. *Spectrochim. Acta, Part A* **2013**, *105*, 326−337.
(20) Vajragupta, O.; Boonchoong, P.; Watanabe, H.; Tohda, M.; Kummasud, N.; Sumanont, Y. Manganese complexes of curcumin and its derivatives: evaluation for the radical scavenging ability and neuroprotective activity. *Free Radical Biol. Med.* **2003**, *35*, 1632−1644.
(21) Sumanont, Y.; Murakami, Y.; Tohda, M.; Vajragupta, O.; Watanabe, H.; Matsumoto, K. Effects of Manganese complexes of Curcumin and diacetylcurcumin on Kainic acid-induced neurotoxic responses in the rat hippocampus. *Biol. Pharm. Bull.* **2007**, *30*, 1732−1739.
(22) Mishra, M. K.; Sanphui, P.; Ramamurty, U.; Desiraju, G. R. Solubility-hardness correlation in molecular crystals: Curcumin and sulfathiazole polymorphs. *Cryst. Growth Des.* **2014**, *14*, 3054−3061.
(23) Caruso, F.; Rossi, M.; Benson, A.; Opazo, C.; Freedman, D.; Monti, E.; Gariboldi, M. B.; Shaulky, J.; Marchetti, F.; Pettinari, R.; Pettinari, C. Ruthenium−arene complexes of curcumin: X-ray and density functional theory structure, synthesis, and spectroscopic characterization, *in vitro* antitumor activity, and DNA docking studies of (*p*-cymene) Ru(curcuminato)chloro. *J. Med. Chem.* **2012**, *55*, 1072−1081.
(24) Leung, M. H. M.; Harada, T.; Kee, T. W. Delivery of curcumin and medicinal effects of the copper(II)-curcumin complexes. *Curr. Pharm. Des.* **2013**, *19*, 2070−2083.
(25) Pröhl, M.; Schubert, U. S.; Weigand, W.; Gottschaldt, M. Metal complexes of curcumin and curcumin derivatives for molecular imaging and anticancer therapy. *Coord. Chem. Rev.* **2016**, *307*, 32−41.
(26) Raygada, J. L.; Levine, D. P. Methicillin-resistant *Staphylococcus aureus*: A growing risk in the hospital and in the community. *Am. Health Drug Benefits* **2009**, *2*, 86−95.
(27) Bakthavatsalam, S.; Das Sharma, S.; Sonawane, M.; Thirumalai, V.; Datta, A. A zebrafish model of manganism reveals reversible and treatable symptoms that are independent of neurotoxicity. *Dis. Models Mech.* **2014**, *7*, 1239−1251.
(28) Borsetti, F.; Dal Piaz, F.; D'Alessio, F.; Stefan, A.; Brandimarti, R.; Sarkar, A.; Datta, A.; Montón Silva, A.; den Blaauwen, T.; Alberto, M.; Spisni, E.; Hochkoeppler, A. Manganese is a *Deinococcus radiodurans* growth limiting factor in rich culture medium. *Microbiology* **2018**, *164*, 1266−1275.
(29) Nakamoto, K. *Infrared and Raman spectra of inorganic and coordination compounds, Part A: Theory and Applications in Inorganic Chemistry*, 6th ed.; Wiley-Interscience: New York, 2009.
(30) Deb, P.; Ghose, M.; Sepay, N.; Maiti, S.; Mukherjea, K. K. Synthesis, characterization, theoretical simulation, and DNA-nuclease activity of a newly synthesized Mn−oximato complex. *J. Coord. Chem.* **2018**, *71*, 3250−3265.
(31) Mary, C. P. V.; Vijayakumar, S.; Shankar, R. Metal chelating ability and antioxidant properties of Curcumin-metal complexes - A DFT approach. *J. Mol. Graphics Modell.* **2018**, *79*, 1−14.
(32) Go, Y.-M.; Jones, D. P. Redox Compartmentalization in eukaryotic cells. *Biochim. Biophys. Acta* **2008**, *1780*, 1273−1290.
(33) Das, P.; Bhattacharya, D.; Karmakar, P.; Das, S. Influence of ionic strength on the interaction of THA and its Cu(II) complex with DNA helps to explain studies on various breast cancer cells. *RSC Adv.* **2015**, *5*, 73099−73111.
(34) Ghosh, S.; Kundu, P.; Paul, B. K.; Chattopadhyay, N. Binding of an anionic fluorescent probe with calf thymus DNA and effect of salt on the probe-DNA binding: a spectroscopic and molecular docking investigation. *RSC Adv.* **2014**, *4*, 63549−63558.
(35) Saha, M.; Singha, S.; Chakraborty, M.; Mazumdar, S.; Kumar, S.; Karmakar, P.; Das, S. Characterization of a MnII complex of alizarin suggests attributes explaining a superior anticancer activity: A comparison with anthracycline drugs. *Polyhedron* **2019**, *173*, 114104.
(36) Guin, P. S.; Mandal, P. C.; Das, S. The binding of a hydroxy-9,10-anthraquinone Cu^{II} complex to calf thymus DNA: Electrochemistry and UV/Vis spectroscopy. *ChemPlusChem* **2012**, *77*, 361−369.
(37) Das, P.; Jain, C. K.; Dey, S. K.; Saha, R.; Chowdhury, A. D.; Roychoudhury, S.; Kumar, S.; Majumder, H. K.; Das, S. Synthesis, crystal structure, DNA interaction and *in vitro* anticancer activity of a Cu(II) complex of purpurin: dual poison for human DNA topoisomerase I and II. *RSC Adv.* **2014**, *4*, 59344−59357.
(38) Mandal, B.; Singha, S.; Dey, S. K.; Mazumdar, S.; Mondal, T. K.; Karmakar, P.; Kumar, S.; Das, S. Synthesis, crystal structure from PXRD of a $Mn^{II}(purp)_2$ complex, interaction with DNA at different temperatures and pH and lack of stimulated ROS formation by the complex. *RSC Adv.* **2016**, *6*, 51520−51532.

https://dx.doi.org/10.1021/acsomega.9b04079
ACS Omega 2020, 5, 16342−16357

(39) Saha, M.; Nandy, P.; Chakraborty, M.; Das, P.; Das, S. The importance of pK_a in an analysis of the interaction of compounds with DNA. *Biophys. Chem.* **2018**, *236*, 15−21.
(40) Scatchard, G. The attractions of proteins for small molecules and ions. *Ann. N.Y. Acad. Sci.* **1949**, *51*, 660−672.
(41) Huang, C.-H.; Mong, S.; Crooke, S. T. Interactions of a new antitumor antibiotic BBM-928A with deoxyribonucleic acid. Bifunctional intercalative binding studied by fluorometry and viscometry. *Biochemistry* **1980**, *19*, 5537−5542.
(42) Ardan, T.; Kovačeva, J.; Čejková, J. Comparative histochemical and immunohistochemical study on xanthine oxidoreductase/xanthine oxidase in mammalian corneal epithelium. *Acta Histochem.* **2004**, *106*, 69−75.
(43) Hille, R.; Hall, J.; Basu, P. The mononuclear molybdenum enzymes. *Chem. Rev.* **2014**, *114*, 3963−4038.
(44) Lyngsie, G.; Krumina, L.; Tunlid, A.; Persson, P. Generation of hydroxyl radicals from reactions between a dimethoxyhydroquinone and iron oxide nanoparticles. *Sci. Rep.* **2018**, *8*, 10834.
(45) Gligorovski, S.; Strekowski, R.; Barbati, S.; Vione, D. Environmental implications of hydroxyl radicals ($^{\bullet}OH$). *Chem. Rev.* **2015**, *115*, 13051−13092.
(46) Thomas, C.; Mackey, M. M.; Diaz, A. A.; Cox, D. P. Hydroxyl radical is produced via the Fenton reaction in submitochondrial particles under oxidative stress: Implications for diseases associated with iron accumulation. *Redox Rep.* **2009**, *14*, 102−108.
(47) Gutteridge, J. M. C.; Halliwell, B. The deoxyribose assay: an assay both for 'free' hydroxyl radical and for site-specific hydroxyl radical production. *Biochem. J.* **1988**, *253*, 932−933.
(48) Luqman, S.; Kumar, R. Importance of deoxyribose degradation assay for evaluating hydroxyl radical scavenging activity of punica extract. *Int. J. Food Prop.* **2012**, *15*, 942−948.
(49) Joshi, S.; Mumtaz, S.; Singh, J.; Pasha, S.; Mukhopadhyay, K. Novel miniature membrane active lipopeptidomimetics against planktonic and biofilm embedded methicillin-resistant *Staphylococcus aureus*. *Sci. Rep.* **2018**, *8*, 1021.
(50) Singh, M.; Mukhopadhyay, K. C-Terminal amino acids of alpha-melanocyte-stimulating hormone are requisite for its antibacterial activity against *Staphylococcus aureus*. *Antimicrob. Agents Chemother.* **2011**, *55*, 1920−1929.
(51) Ouberai, M.; El Garch, F.; Bussiere, A.; Riou, M.; Alsteens, D.; Lins, L.; Baussanne, I.; Dufrêne, Y. F.; Brasseur, R.; Decout, J.-L.; Mingeot-Leclercq, M.-P. The *Pseudomonas aeruginosa* membranes: A target for a new amphiphilic aminoglycoside derivative? *Biochim. Biophys. Acta, Biomembr.* **2011**, *1808*, 1716−1727.
(52) Kumar, P.; Kandi, S. K.; Manohar, S.; Mukhopadhyay, K.; Rawat, D. S. Monocarbonyl Curcuminoids with Improved Stability as Antibacterial Agents against *Staphylococcus aureus* and Their Mechanistic Studies. *ACS Omega* **2019**, *4*, 675−687.
(53) Koo, S.-P.; Bayer, A. S.; Yeaman, M. R. Diversity in Anti staphylococcal Mechanisms among Membrane-Targeting Antimicrobial Peptides. *Infect. Immun.* **2001**, *69*, 4916−4922.
(54) Xiong, Y.-Q.; Yeaman, M. R.; Bayer, A. S. *In Vitro* Antibacterial Activities of Platelet Microbicidal Protein and Neutrophil Defensin against *Staphylococcus aureus* Are Influenced by Antibiotics Differing in Mechanism of Action. *Antimicrob. Agents Chemother.* **1999**, *43*, 1111−1117.
(55) Glenn, J. K.; Akileswaran, L.; Gold, M. H. Mn(II) oxidation is the principal function of the extracellular Mn-peroxidase from phanerochaete chrysosporium. *Arch. Biochem. Biophys.* **1986**, *251*, 688−696.
(56) Tønnesen, H. H.; Másson, M.; Loftsson, T. Studies of curcumin and curcuminoids. XXVII. Cyclodextrin complexation: solubility, chemical and photochemical stability. *Int. J. Pharm.* **2002**, *244*, 127−135.
(57) Bernabé-Pineda, M.; Ramírez-Silva, M. T.; Romero-Romo, M.; González-Vergara, E.; Rojas-Hernández, A. Determination of acidity constants of curcumin in aqueous solution and apparent rate constant of its decomposition. *Spectrochim. Acta, Part A* **2004**, *60*, 1091−1097.
(58) Priyadarsini, K. The Chemistry of Curcumin: From Extraction to Therapeutic Agent. *Molecules* **2014**, *19*, 20091−20112.
(59) Das, P.; Jain, C. K.; Roychoudhury, S.; Majumder, H. K.; Das, S. Design, Synthesis and *in vitro* Anticancer Activity of a Cu(II) Complex of Carminic Acid: A Novel Small Molecule Inhibitor of Human DNA Topoisomerase I and Topoisomerase II. *ChemistrySelect* **2016**, *1*, 6623−6631.
(60) Mukherjee Chatterjee, S.; Jain, C. K.; Singha, S.; Das, P.; Roychoudhury, S.; Majumder, H. K.; Das, S. Activity of Co^{II}-Quinalizarin: A novel analogue of anthracycline-based anticancer agents targets human DNA topoisomerase, whereas quinalizarin itself acts via formation of semiquinone on acute lymphoblastic leukemia MOLT-4 and HCT 116 cells. *ACS Omega* **2018**, *3*, 10255−10266.
(61) (a) Liu, T.; Zhang, H.-X.; Xia, B.-H. Theoretical studies on structures and spectroscopic properties of a series of novel cationic [trans-(C/N)2Ir(PH3)2]+ (C/N = ppy, bzq, ppz, dfppy). *J. Phys. Chem. A* **2007**, *111*, 8724−8730. (b) Zhou, X.; Zhang, H.-X.; Pan, Q.-J.; Xia, B.-H.; Tang, A.-C. Theoretical Studies of the Spectroscopic Properties of [Pt(trpy)C⋮CR]+(trpy = 2,2′,6′,2″-Terpyridine; R = H, CH2OH, and C6H5). *J. Phys. Chem. A* **2005**, *109*, 8809−8818. (c) Zhou, X.; Ren, A.-M.; Feng, J.-K. Theoretical studies on the ground states in (M=Fe, Ru, Os) and excited states in using density functional theory. *J. Organomet. Chem.* **2005**, *690*, 338−347.
(62) Frisch, M. J.; Trucks, G. W.; Schlegel, H. B.; Scuseria, G. E.; Robb, M. A.; Cheeseman, J. R.; Scalmani, G.; Barone, V.; Mennucci, B.; Petersson, G. A.; Nakatsuji, H.; Caricato, M.; Li, X.; Hratchian, H. P.; Izmaylov, A. F.; Bloino, J.; Zheng, G.; Sonnenberg, J. L.; Hada, M.; Ehara, M.; Toyota, K.; Fukuda, R.; Hasegawa, J.; Ishida, M.; Nakajima, T.; Honda, Y.; Kitao, O.; Nakai, H.; Vreven, T.; Montgomery, J. A., Jr.; Peralta, J. E.; Ogliaro, F.; Bearpark, M.; Heyd, J. J.; Brothers, E.; Kudin, K. N.; Staroverov, V. N.; Kobayashi, R.; Normand, J.; Raghavachari, K.; Rendell, A.; Burant, J. C.; Iyengar, S. S.; Tomasi, J.; Cossi, M.; Rega, N.; Millam, J. M.; Klene, M.; Knox, J. E.; Cross, J. B.; Bakken, V.; Adamo, C.; Jaramillo, J.; Gomperts, R.; Stratmann, R. E.; Yazyev, O.; Austin, A. J.; Cammi, R.; Pomelli, C.; Ochterski, J. W.; Martin, R. L.; Morokuma, K.; Zakrzewski, V. G.; Voth, G. A.; Salvador, P.; Dannenberg, J. J.; Dapprich, S.; Daniels, A. D.; Farkas, Ö.; Foresman, J. B.; Ortiz, J. V.; Cioslowski, J.; Fox, D. J. *Gaussian 09*, Revision A.1; Gaussian, Inc.; Wallingford, CT, 2009.
(63) Becke, A. D. Density-functional exchange-energy approximation with correct asymptotic behavior. *Phys. Rev. A: At., Mol., Opt. Phys.* **1988**, *38*, 3098.
(64) Leung, K.; Rempe, S. B.; Schultz, P. A.; Sproviero, E. M.; Batista, V. S.; Chandross, M. E.; Medforth, C. J. Density functional theory and DFT+U study of transition metal porphines adsorbed on Au(111) surfaces and effects of applied electric fields. *J. Am. Chem. Soc.* **2006**, *128*, 3659−3668.
(65) Lee, C.; Yang, W.; Parr, R. G. Development of the Colle-Salvetti correlation-energy formula into a functional of the electron density. *Phys. Rev. B: Condens. Matter Mater. Phys.* **1988**, *37*, 785−789.
(66) (a) Hay, P. J.; Wadt, W. R. *Ab initio* effective core potentials for molecular calculations. Potentials for the transition metal atoms Sc to Hg. *J. Chem. Phys.* **1985**, *82*, 270−283. (b) Handy, N. C.; Schaefer, H. F. On the evaluation of analytic energy derivatives for correlated wave functions. *J. Chem. Phys.* **1984**, *81*, 5031−5033. (c) Nicklass, A.; Dolg, M.; Stoll, H.; Preuss, H. *Ab initio* energy-adjusted pseudopotentials for the noble gases Ne through Xe: Calculation of atomic dipole and quadrupolepolarizabilities. *J. Chem. Phys.* **1995**, *102*, 8942−8952.
(67) Yanai, T.; Tew, D. P.; Handy, N. C. A new hybrid exchange-correlation functional using the coulomb-attenuating method (CAM-B3LYP). *Chem. Phys. Lett.* **2004**, *393*, 51−57.
(68) O'boyle, N. M.; Tenderholt, A. L.; Langner, K. M. Cclib: A library for package-independent computational chemistry algorithms. *J. Comput. Chem.* **2008**, *29*, 839−845.
(69) Aggarwal, S.; Ichikawa, H.; Takada, Y.; Sandur, S. K.; Shishodia, S.; Aggarwal, B. B. Curcumin (Diferuloylmethane) Down-Regulates Expression of Cell Proliferation and Antiapoptotic and Metastatic Gene Products through Suppression of IκBα Kinase and Akt Activation. *Mol. Pharmacol.* **2006**, *69*, 195−206.

https://dx.doi.org/10.1021/acsomega.9b04079
ACS Omega 2020, 5, 16342−16357

(70) Robak, J.; Gryglewski, R. J. Flavonoids are scavengers of superoxide anions. *Biochem. Pharmacol.* **1988**, *37*, 837−841.
(71) Mishra, B.; Priyadarsini, K. I.; Kumar, M. S.; Unnikrishnan, M. K.; Mohan, H. Effect of O-glycosilation on the antioxidant activity and free radical reactions of a plant flavonoid, chrysoeriol. *Bioorg. Med. Chem.* **2003**, *11*, 2677−2685.
(72) Singh, M.; Gadepalli, R.; Dhawan, B.; Mukhopadhyay, K. Combination of alpha-melanocyte stimulating hormone with conventional antibiotics against methicillin resistant *Staphylococcus aureus*. *PLoS One* **2013**, *8*, No. e73815.
(73) Hsu, C.-H.; Chen, C.; Jou, M. L.; Lee, A. Y. L.; Lin, Y. C.; Yu, Y. P.; Wu, S. H. Structural and DNA-binding studies on the bovine antimicrobial peptide, indolicidin: Evidence for multiple conformations involved in binding to membranes and DNA. *Nucleic Acids Res.* **2005**, *33*, 4053−4064.
(74) Singh, J.; Joshi, S.; Mumtaz, S.; Maurya, N.; Ghosh, I.; Khanna, S.; Natarajan, V. T.; Mukhopadhyay, K. Enhanced Cationic Charge is a Key Factor in Promoting Staphylocidal Activity of α-Melanocyte Stimulating Hormone via Selective Lipid Affinity. *Sci. Rep.* **2016**, *6*, 31492.

https://dx.doi.org/10.1021/acsomega.9b04079
ACS Omega 2020, 5, 16342−16357